

Graphical Models with Attention for Context-Specific Independence and an Application to Perceptual Grouping

Guangyao Zhou, Wolfgang Lehrach, Antoine Dedieu, Miguel Lázaro-Gredilla, Dileep George

Vicarious AI

{stannis, wolfgang, antoine, miguel, dileep}@vicarious.com

Abstract

Discrete undirected graphical models, also known as Markov Random Fields (MRFs), can flexibly encode probabilistic interactions of multiple variables, and have enjoyed successful applications to a wide range of problems. However, a well-known yet little studied limitation of discrete MRFs is that they cannot capture context-specific independence (CSI). Existing methods require carefully developed theories and purpose-built inference methods, which limit their applications to only small-scale problems. In this paper, we propose the Markov Attention Model (MAM), a family of discrete MRFs that incorporates an *attention* mechanism. The *attention* mechanism allows variables to dynamically *attend* to some other variables while *ignoring* the rest, and enables capturing of CSIs in MRFs. A MAM is formulated as an MRF, allowing it to benefit from the rich set of existing MRF inference methods and scale to large models and datasets. To demonstrate MAM’s capabilities to capture CSIs at scale, we apply MAMs to capture an important type of CSI that is present in a symbolic approach to recurrent computations in perceptual grouping. Experiments on two recently proposed synthetic perceptual grouping tasks and on realistic images demonstrate the advantages of MAMs in sample-efficiency, interpretability and generalizability when compared with strong recurrent neural network baselines, and validate MAM’s capabilities to efficiently capture CSIs at scale.

Introduction

Context-specific independence Probabilistic Graphical Models (PGMs) compactly encode conditional independence information in multivariate distributions with graph-based representations. However, a well-known limitation of PGMs is that they cannot capture context-specific independence (CSI) (Boutilier et al. 1996; Friedman and Goldszmidt 1998; Fridman 2003; Nyman et al. 2014), i.e. independence relationships that only hold for certain joint variable states. Many past works (Boutilier et al. 1996; Friedman and Goldszmidt 1998; Poole and Zhang 2003) focus on encoding CSIs for directed graphical models, also known as Bayesian Networks (BNs). Discrete undirected graphical models, also known as Markov Random Fields (MRFs), have enjoyed successful applications to a wide range of problems (Koller and Friedman 2009). Yet exploiting CSI in discrete MRFs has received relatively little attention. Existing methods typically augment MRFs, e.g. by introducing special node-

valued random variables (Fridman 2003), or by annotating graph edges (Nyman et al. 2014). However, the augmented models are no longer MRFs, and as a result require carefully developed theories and purpose-built inference methods. The lack of standard tooling has so far limited their applications to only small-scale problems.

In this paper, we propose the Markov Attention Model (MAM), a family of discrete MRFs that incorporates an *attention* mechanism to flexibly capture CSIs in undirected models. The *attention* mechanism allows variables to dynamically (i.e. in a context-specific way) *attend to* (i.e. conditionally depend on) some other variables while *ignoring* (i.e. being conditionally independent of) the rest. We implement the attention mechanism with higher-order factors (HOFs) and discrete attention variables. Each attention variable is connected to two regular variables, and encodes a) information about the joint states of the two connected regular variables with a set of ON states; and b) CSI between the two regular variables with a special OFF state. The HOFs enforce consistency between ON attention variables and their connected regular variables, and capture CSIs by turning certain attention variables OFF for given regular variable states.

Despite the introduction of attention variables, existing MRF inference methods are readily applicable to MAMs due to its formulation as a discrete MRF. In our experiments, we leverage this fact to develop efficient inference methods for MAMs based on max-product belief propagation (MPBP) (Weiss and Freeman 2001), resulting in orders of magnitude improvements in scalability. MAM provides a general and efficient approach for capturing CSIs using MRFs, with potential applications to myriad discrete data, e.g. gene regulatory networks (Shmulevich et al. 2002), word sense disambiguation (Navigli 2009), and a symbolic approach to recurrent computations for perceptual grouping.

Perceptual grouping and recurrent computations To demonstrate the capabilities of MAM at scale, we focus on modeling recurrent computations in perceptual grouping using MAM. Perceptual grouping puts multiple parts into a whole, and is a fundamental component of visual intelligence. Inspired by evidence (Roelfsema 2006; Roelfsema and Houtkamp 2011; Gilbert and Li 2013) on the importance of top-down and lateral *recurrent connections* (Lamme, Supèr, and Spekreijse 1998; Sporns and Zwi 2004) for perceptual grouping, recent computational models (Linsley

et al. 2018; Kim et al. 2020) incorporate *recurrent computations* using recurrent neural networks (RNNs), and achieve state-of-the-art (SOTA) performance when compared with purely feedforward convolutional neural networks (CNNs). However, as we show in our experiments, they suffer from the now well-known limitations of deep neural networks (DNNs) (Serre 2019; Marcus 2018): they require a large amount of training data, are hard to interpret, and do not generalize well to novel setups.

It has long been postulated (Hinton 1990; Bader and Hitzler 2005; Garnelo and Shanahan 2019; Marcus 2020; Garcez and Lamb 2020) that an effective approach for overcoming such limitations involves high-level, abstract reasoning with symbol-like entities (e.g. abstract *objects* and *object parts*). In this paper, we take such a symbolic approach, and build probabilistic models of abstract object-/object parts and their interactions. We identify an important type of CSI that is present in such models: object parts are conditionally independent when they belong to different objects. We show how we can formulate MAMs to flexibly capture such CSIs and build compact probabilistic models that are sample-efficient, interpretable and generalizable.

Scope Our MAMs for perceptual grouping operate on the symbolic level, and as a result face the symbol grounding problem (Harnad 1990). Since our goal is to demonstrate MAM’s capabilities to capture CSIs at scale, we experiment with two recently proposed synthetic perceptual grouping tasks with binary images, the pathfinder challenge and the cABC challenge (Linsley et al. 2018; Kim et al. 2020), for which we can solve the symbol grounding problem with a *sparsifier*. A sparsifier is a simple binary MRF. It connects the perceptual representations (the binary images) and the symbolic representations (the object parts), and enables learning of MAMs directly from binary images (e.g. **Fig. 3**).

Although the two perceptual grouping tasks are synthetic in nature, they are by no means simple. In fact, sophisticated CNN baselines using ResNet (Ronneberger, Fischer, and Brox 2015) and U-net (Ronneberger, Fischer, and Brox 2015) struggle on these challenges, and novel RNNs are needed to satisfactorily solve the challenges (Kim et al. 2020). In addition, SOTA transformers (Tay et al. 2020; Xiong et al. 2021; Lee-Thorp et al. 2021; Moskvichev and Liu 2021) were recently applied to lower-resolution variations of the pathfinder challenge, but perform poorly when compared with MAMs or our RNN baselines (Kim et al. 2020). Nevertheless, as a proof-of-concept, we show that, with some manual design, we can easily apply MAMs trained with rich prior information on singulated objects in the form of object masks to realistic images. The additional experiment hints at MAM’s potential in fields like robotics (Sünderhauf et al. 2018), where we benefit from structured probabilistic models that can be trained in a sample-efficient way while taking into account available rich prior information (e.g. 3D object models). However, MAM is not intended as a replacement for existing methods in situations with much training data but no rich prior information.

Contributions The main contributions of the paper are:

1. We propose MAM, a family of discrete MRFs that flexi-

bly captures CSIs in MRFs. Since a MAM is formulated as a discrete MRF, no additional theory is needed, and existing MRF inference methods are readily applicable. This allows MAMs to scale to large models and datasets.

2. We identify an important type of CSI in a symbolic approach to recurrent computations for perceptual grouping, and use this as a test case to demonstrate MAM’s capabilities to capture CSIs in MRFs at scale.
3. We apply MAMs to two recently proposed synthetic perceptual grouping tasks. We develop efficient learning of MAMs directly from binary images using large-scale datasets (e.g. with 900K 300×300 images), and scalable approximate inference procedures based on MPBP to test large MAMs. Experimental results demonstrate MAMs’ advantages when compared with SOTA RNN baselines: a) MAMs are more sample-efficient, and order(s) of magnitude more so in challenging situations, b) MAMs give interpretable and semantically meaningful decodings, c) MAMs exhibit high generalizability across setups, while RNNs struggle or completely fail to generalize.
4. We additionally demonstrate MAMs’ power and flexibility by applying MAMs trained with rich prior information on singulated objects to realistic images.

Presentation style For readability, we focus on intuitive descriptions in the main text, and defer the formal, rigorous description of all models and methods to the supplementary.

Background and related works

Context-specific independence For BNs, CSI brings more compact encoding and significant inference speedups (Boutilier et al. 1996), and allows learning of BN models that better emulate the real complexity of the interactions present in the data (Friedman and Goldszmidt 1998). However, exploiting CSI for MRFs has received relatively little attention (Fridman 2003; Nyman et al. 2014). As a simple example for CSI in MRFs, consider the following gene network from (Fridman 2003):

The protein product pA of gene A induces expression of gene B. Compound C, when present, modifies pA. The modified protein is unable to regulate B directly but can induce expression of gene D. Genes B and D are corepressive (pB inhibits expression of D; pD inhibits expression of B).

Denote by $X_A, X_B, X_D \in \{0, 1\}$ the expression levels of genes A, B, D, and by $X_C \in \{0, 1\}$ the presence/absence of compound C. The network contains obvious CSIs: X_A, X_B are only conditionally independent when $X_C = 1$ while X_A, X_D are only conditionally independent when $X_C = 0$. Despite such CSIs, (Fridman 2003) shows that every pair of variables in the MRF modeling this network are directly dependent, and the MRF is *fully connected* (**Fig. 1[left]**).

In (Fridman 2003), the author captures CSIs by replacing X_C with a node-valued random variable taking values in $\{X_B, X_D\}$ to represent which gene is directly regulated by A, but has to carefully establish the Markov property and develop inference methods based on a customized Gibbs sampler. In (Nyman et al. 2014), the authors annotate graph

edges to capture CSIs, but the theory and application are restricted to a simplistic family of *decomposable* models.

Perceptual grouping Probabilistic methods for problems related to perceptual grouping have a rich history in computer vision (Ren, Fowlkes, and Malik 2005, 2006; Hoiem et al. 2007; He and Yuille 2010; Silberman et al. 2014). They usually model *concrete entities* (e.g. boundaries and surfaces) using RGB and depth information. In this paper, we explore an alternative, symbolic approach where we build probabilistic models of abstract objects/object parts and their interactions. This symbolic approach reveals an important type of CSI, making it a suitable test case for MAM.

Recurrent computations using RNNs Motivated by the abundant recurrent connections in the visual cortex, several recent computational models (Kubilius et al. 2019; Liang and Hu 2015; Liao and Poggio 2016; Spoerer, McClure, and Kriegeskorte 2017; Zamir et al. 2017; Nayebi et al. 2018; Linsley et al. 2018; Kim et al. 2020) incorporate recurrent computations using RNNs. They outperform purely feedforward CNNs with more compact models/fewer parameters, yet suffer from well-known limitations of DNNs in sample-efficiency, interpretability and generalizability. There have been significant efforts in the RNN literature on addressing the above limitations. In particular, several recent works (Goyal et al. 2020; Mittal et al. 2020; Goyal et al. 2021) explore ideas similar to our identified CSI for perceptual grouping for better generalizability. In this paper, we demonstrate how MAM can implement such CSI within an MRF, and obtain better sample-efficiency and interpretability, in addition to improved generalizability.

Attention Attention was first introduced in deep learning (Bahdanau, Cho, and Bengio 2014; Mnih et al. 2014). It has subsequently found great success in both natural language processing (Vaswani et al. 2017; Galassi, Lippi, and Torroni 2020) and computer vision (Han et al. 2020; Khan et al. 2021), and plays an important role in many graph neural networks (Veličković et al. 2017; Lee et al. 2019). In this paper, we reinterpret attention as a mechanism for implementing CSIs in MRFs, and demonstrate its usefulness in symbolic recurrent computations for perceptual grouping.

Max-product belief propagation MPBP is a message-passing based inference method for approximately computing the maximum-a-posteriori (MAP) state in a PGM. It is highly scalable since it involves only parallelizable local computations. We use MPBP in the log domain with damping (Cohen and Zivan 2017) for inference in all our models.

Compositional object models Our symbolic approach to perceptual grouping is similar in spirit to compositional object models, i.e. hierarchical probabilistic models of objects/object parts. Some past works (Jin and Geman 2006; Zhu and Mumford 2007; Lake, Salakhutdinov, and Tenenbaum 2015) rely on less scalable Markov Chain Monte Carlo or heuristic methods for inference. Others (George et al. 2017; Chua and Felzenszwalb 2020) similarly adopt PGMs with belief propagation for inference. Among these, the recursive cortical network (George et al. 2017) is closely related to our object-specific MAM for cABC, but lacks the capacity for object-agnostic modeling (e.g. for pathfinder). Probabilistic scene grammars (Chua and Felzenszwalb 2020) model top-

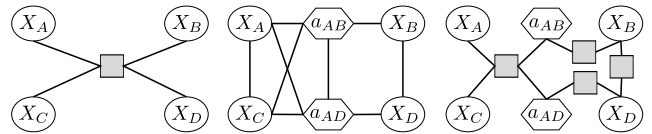


Figure 1: MRFs for the gene network from (Fridman 2003). [Left] Factor graph for the MRF modeling the network. The shaded square represents the single HOF. [Center] Graph of conditional independence relationships for the MAM modeling the network. [Right] Factor graph for the MAM modeling the network. Shaded squares represent factors.

down interactions using grammar production rules, but lack proper modeling of lateral interactions.

Methods

Markov Attention Model

Revisiting the gene network example We start by showing how we can formulate a MAM to encode the obvious CSIs in the gene network example from (Fridman 2003). We adopt the standard factor graph (FG) representation (Kschischang, Frey, and Loeliger 2001) for discrete MRFs. An FG is a bipartite graph connecting variables to factors.

To capture CSIs, we introduce two binary attention variables $a_{AB}, a_{AD} \in \{\text{ON}, \text{OFF}\}$, one for each pair of variables with CSI. Intuitively, the attention variables indicate whether A directly regulates B, D. The MAM modeling the gene network is a discrete MRF on 4 regular variables X_A, X_B, X_C, X_D and the two introduced attention variables. We visualize its graph in **Fig. 1[center]** and its FG in **Fig. 1[right]**. The MAM is specified by 4 factors:

1. A HOF involving X_A, X_C, a_{AB}, a_{AD} . It models A, C interactions and captures the CSIs with 4 joint states:
 - (a) $X_A = 0, X_C = 0, a_{AB}$ is OFF, a_{AD} is OFF.
 - (b) $X_A = 0, X_C = 1, a_{AB}$ is OFF, a_{AD} is OFF.
 - (c) $X_A = 1, X_C = 0, a_{AB}$ is ON, a_{AD} is OFF.
 - (d) $X_A = 1, X_C = 1, a_{AB}$ is OFF, a_{AD} is ON.
2. A factor involving a_{AB}, X_B . It promotes $X_B = 1$ when A directly regulates B (a_{AB} is ON), and gives 0 potential (in log domain) when A does not (a_{AB} is OFF).
3. A factor involving a_{AD}, X_D , similar to the above.
4. A factor involving X_B, X_D , modeling corepressiveness.

The ON state of an attention variable encodes information about joint states of its connected regular variables (e.g. a_{AB} is ON means $X_A = 1$ and X_B is likely 1). Factors involving regular and attention variables enforce consistency between regular variables and ON attention variables (e.g. factor 1 enforces $X_A = 1$ when any connected attention variable is ON, and factor 2 enforces X_B is likely 1 when a_{AB} is ON), and models CSIs by turning certain attention variables OFF (e.g. joint states (c), (d) in factor 1). In what follows, we present the general formulation of MAM, and demonstrate in later

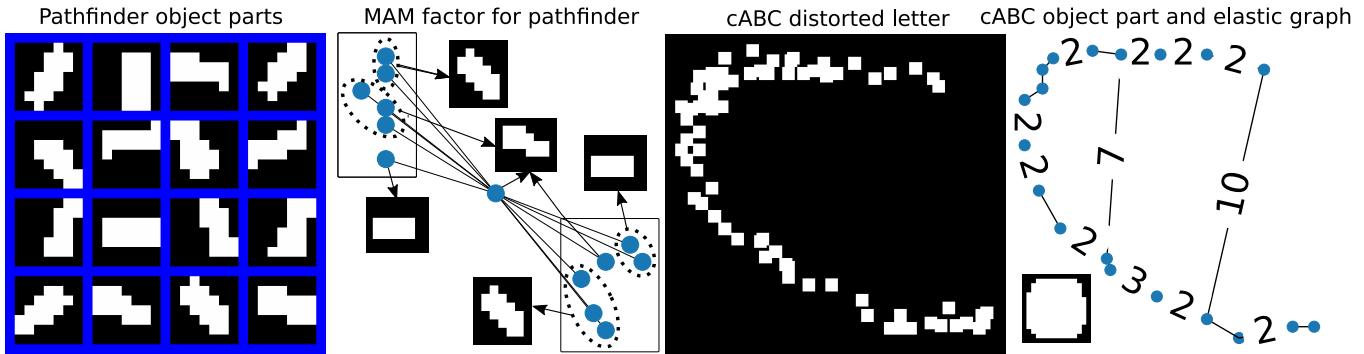


Figure 2: [Left] 16 learned object parts for the pathfinder challenge. [Center left] Top 12 (out of more than 800) possible contour continuations for a given object part. Blue dots represent object parts. Each rectangle represents contour continuations on one side. Dotted circles represent the same type of object parts at different locations. Arrows point to visualizations of the corresponding object parts. [Center right] A noisy, distorted letter from the cABC challenge. [Right] A single learned object part for the cABC challenge, and the extracted elastic graph for the center right letter. Visualized numbers are the perturb radiuses associated with the edges (elastic constraints). Edges with no associated numbers have perturb radius 1.

sections how we can formulate, learn and apply MAMs to capture CSIs, with perceptual grouping as an example.

General formulation Given a FG, we say two variables are ψ -connected if there exists a factor that connects to both variables. A MAM is defined as a discrete MRF with two types of variables and additional connectivity constraints:

1. A variable is either a regular or an attention variable.
2. An attention variable is ψ -connected to exactly two regular variables. We denote the attention variable that is ψ -connected to the regular variables x_u, x_v by $a_{\{x_u, x_v\}}$.
3. A factor that is connected to an attention variable is also connected to exactly one regular variable that is ψ -connected to the attention variable.

For the attention variables, we additionally designate ON states encoding information about joint states of the two ψ -connected regular variables, and special OFF states encoding CSIs. The factors model regular variable interactions, enforce consistency between regular and attention variables, and capture CSIs with OFF attention variables.

Applying MAMs to perceptual grouping

We take a symbolic approach to perceptual grouping, and build probabilistic models of abstract objects/object parts and their interactions. Inspired by the importance of top-down and lateral recurrent connections, we focus on implementing two types of *symbolic recurrent computations*: a) modeling part-whole relationships with top-down parent/children interactions, and b) modeling object parts co-occurrences with lateral contextual interactions. We introduce binary *part variables* as the regular variables in our MRFs to model the presence/absence of objects/object parts.

We consider generic and reusable object parts, i.e. object parts that can belong to many different objects, and interact with many object parts. Modeling such interactions with an MRF on part variables quickly becomes infeasible due to large HOFs with exponential number of states. However,

we observe an important type of CSI: object parts are conditionally independent when they belong to different objects. We can exploit such CSI to build more compact models. For example, if we know an object part interacts with two other object parts (e.g. as part of a closed contour), after identifying which two object parts it interacts with, it becomes independent of any other object parts.

We can easily formulate MAMs to capture such CSI. We introduce binary attention variables, one for each pair of interacting part variables. An ON attention variable implies both connected part variables are ON, while an OFF attention variable encodes CSI between the two connected part variables. We introduce HOFs, one for each part variable. A HOF involves its associated part variable and all its connected attention variables. It enforces consistency between the part and attention variables: the part variable should be ON when at least one of its connected attention variable is ON. It encodes CSI by turning ON a sparse (but non-empty) set of attention variables when the part variable is ON. The sparse set of ON attention variables models both part-whole relationships and object parts co-occurrences, while also serves as the context for CSI with other part variables.

We additionally incorporate invariance by partitioning the set of attention variables connected to a part variable. Each subset models variations in location of an interacting object part. A HOF identifies the sparse set of interactions by picking first a few subsets (a *prototypical interaction pattern*) followed by exactly one attention variable within each subset. See the supplementary for a formal description.

By encoding CSIs, MAMs can focus on modeling essential interactions within single objects, without worrying about multi-object interactions. As we see in our experiments, this translates into compact probabilistic models with superior sample-efficiency and generalizability. MAMs are additionally highly interpretable because of intuitive formulations: from the result of MAP inference, we can read off which objects/object parts are present from ON part variables, and identify which object parts belong to the same ob-

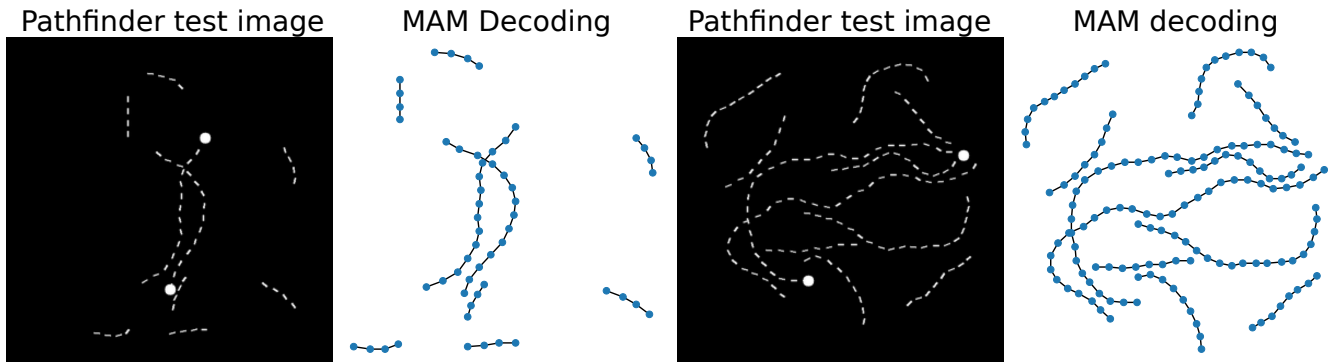


Figure 3: [Left] A *hard* pathfinder test image. [Center left] MAM decoding for the left image. [Center right] An *ultimate* pathfinder test image. [Right] MAM decoding for the center right image.

Table 1: Generalization across difficulties on pathfinder for H-CNN (trained on 900K images) and MAM (trained on 5K images). We follow (Kim et al. 2020) for training H-CNN on *easy*, *medium* and *hard*, but train for $4\times$ longer on *ultimate*. MAM can easily generalize across difficulty levels, while H-CNN completely fails to generalize, despite being trained for longer and on $180\times$ more images. We expect similarly good performances from MAMs trained on *ultimate*, but did not retrain since we only introduce *ultimate* as an additional generalization test.

Train \ Test	Easy		Medium		Hard		Ultimate	
	H-CNN	MAM	H-CNN	MAM	H-CNN	MAM	H-CNN	MAM
Easy	99.47%	98.74%	49.01%	98.65%	49.48%	98.21%	49.88%	97.21%
Medium	45.71%	98.92%	98.02%	99.00%	49.55%	98.77%	49.90%	98.33%
Hard	46.95%	98.92%	48.52%	99.07%	97.60%	98.80%	49.94%	98.42%
Ultimate	29.52%	–	39.67%	–	56.94%	–	79.68%	–

ject from connectivity patterns with ON attention variables.

Symbol grounding with the sparsifier

A sparsifier is a binary MRF containing two different types of variables: a) binary part variables (same as in MAMs) for the presence/absence of object parts, and b) binary pixel variables for pixels in a binary image. We describe an object part by a set of pixels on the image, and consider the object part as a *parent* of its covered pixels. There is one OR factor per pixel variable, which is a HOF that connects the pixel variable and all its parent part variables. The OR factor implements *explaining away* (Wellman and Henrion 1993): the pixel is most likely ON when at least one parent is ON, and most likely OFF when all parents are OFF. See the supplementary for a formal description of the model.

Connecting MAMs with binary images In our experiments, we combine a sparsifier with a MAM to form a probabilistic model for binary images: given a MAM and a binary image, we associate with each part variable in the MAM a set of pixels in the binary image, and combine the HOFs in the MAM with the OR factors in the sparsifier.

Sparsification If we bias each part variable towards OFF, because of *explaining away*, we can use inference with the sparsifier to *sparsify* a binary image, and extract symbolic representations (a sparse set of object parts activations) from perceptual representations (dense binary images). See the supplementary for an illustrative example.

Learning MAMs directly from images As a special case of (?), we can augment a sparsifier to represent the object

parts as a set of binary weight variables. An ON weight variable means the object part covers the corresponding pixel. We can then use joint inference on the part, pixel and weight variables over multiple images, with the weight variables shared convolutionally and across images, to learn object parts directly from images without supervision. In our experiments, we learn MAMs by first learning the object parts on a few training images using the above procedure, before sparsifying training images with the learned object parts to learn the relevant interactions.

Experiments

We develop efficient MPBP updates for the HOFs in MAMs and the sparsifier by exploiting their simple structures, and implement MPBP using *JAX* (Bradbury et al. 2018) with parallel updates of all messages at each iteration to fully leverage the power of modern accelerators like GPUs. See the supplementary for detailed message updating equations. Code is available at <https://github.com/vicariousinc/mam/>.

Pathfinder challenge

Task The pathfinder challenge (Linsley et al. 2018; Kim et al. 2020) uses multiple broken contours as objects, and involves identifying whether two markers are on the same object (Fig. 3). It is expected to be solved by an object-agnostic recurrent routine that groups neighboring low-level visual features according to Gestalt laws. We follow the setups in (Kim et al. 2020), and use the proposed H-CNN, a SOTA RNN that models lateral interactions, as our baseline.

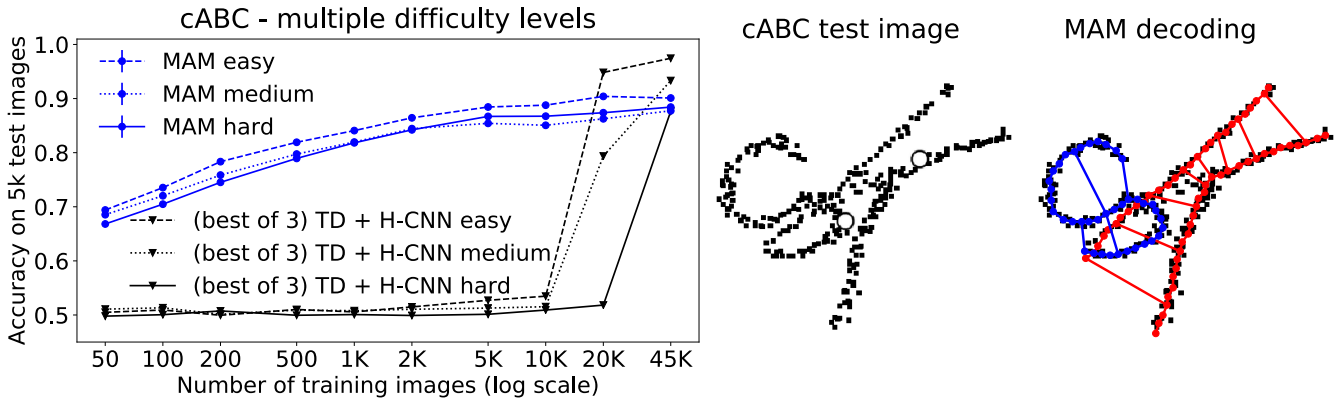


Figure 4: [Left] Evolution of classification accuracy on 5K test images for MAM and TD+H-CNN as the number of training images increase. We average results over three runs for MAMs, but follow (Kim et al. 2020) and report the best result over three runs for TD+H-CNN. Error bars are included for MAMs, but are barely visible due to small accuracy variations across different runs. TD+H-CNN completely fails with less than 20K training images, while MAM performs well above chance with only 50 training images. [Center] cABC test image. [Right] MAM decoding of the center image, showing two elastic graphs matched to the letters.

Table 2: Generalization across difficulties on cABC for TD+H-CNN and MAM (both trained on 45K images).

Train \ Test	Easy		Medium		Hard	
	TD+H-CNN	MAM	TD+H-CNN	MAM	TD+H-CNN	MAM
Easy	97.50%	90.10%	89.60%	87.40%	57.90%	86.36%
Medium	95.00%	89.22%	93.00%	87.74%	61.60%	86.82%
Hard	82.40%	89.00%	82.20%	87.20%	85.60%	88.42%

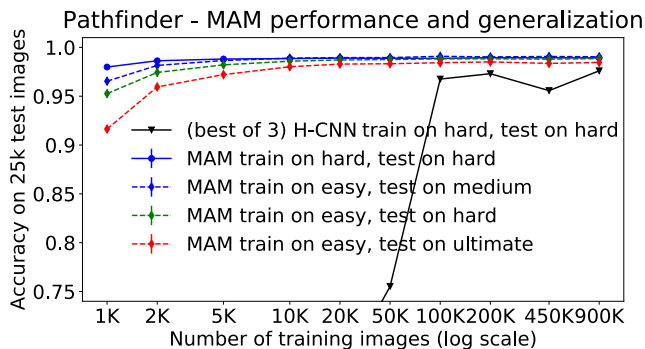


Figure 5: MAM is more sample-efficient than H-CNN on *hard*. MAMs generalize well across difficulties, even with a small number of training images. Notably, an MAM trained on 1K *easy* images gets 91% accuracy on *ultimate*, while an H-CNN trained for 4× longer than (Kim et al. 2020) on 900K *ultimate* images achieves less than 80% accuracy on *ultimate* (Tab. 1).

Embedding Gestalt laws in an object-agnostic MAM

We specify a MAM with 16 types of object parts (Fig. 2[left]), each with possible presence in an $M \times N$ grid of locations. We extract co-occurrences of object parts from data (see **Learning**). Each co-occurrence is applied convolutionally to define a set of attention variables. For a part variable, we partition its associated attention variables into 2 sets to capture possible contour continuations on both sides (Fig. 2[center left]). A HOF is specified by a) a set of proto-

typical interaction patterns enforcing that a contour should continue on one or both sides, and b) the potential in log domain, which penalizes contour termination and encourages the contour to be `OFF` or continue on both sides. We connect the MAM to the image with a sparsifier to model the presence of a variable number of broken contours.

Learning We can fully specify the object-agnostic MAM by extracting a set of co-occurrences of object parts from data. We achieve this by sparsifying individual broken contours (available as part of the data generation process) with the sparsifier, using 16 object parts learned from 10 images (Fig. 2[left]). For each individual broken contour, we obtain sparse object parts activations from MPBP decoding, and heuristically derive the co-occurrences of object parts.

Inference Due to the clean data in the pathfinder challenge, we aggressively prune part and attention variables, by sparsifying a given test image and keeping only the activated part variables and the associated attention variables. We apply MPBP to the pruned MAM for decoding and classification. For images with well-separated contours, this pruning alone can already interpret and classify the images well. However, subsequent inference with MAM helps develop valid interpretations in challenging situations with close or crossing contours (e.g. Fig. 3), and improve classification.

Results We follow (Kim et al. 2020) and experiment with 3 difficulty levels, *easy*, *medium*, *hard*. Although (Kim et al. 2020) used 900K images for all levels, empirically we find that H-CNN can achieve good performance with 1K images

for *easy*, and 2K images for *medium*. On *hard*, the most interesting level, **Fig. 5** shows the additional sample-efficiency of MAM compared to H-CNN: H-CNN struggles even with 50K training images, while MAM achieves close to perfect accuracy with 1K training images. MAM additionally provides semantically meaningful interpretations of the image as multiple contours (e.g. **Fig. 3**). **Fig. 5** and **Tab. 1** show MAM’s superior generalizability. MAMs trained with only 1K images can easily generalize, while H-CNNs trained on $900\times$ more images still completely fail. As an additional and more interesting generalization test, we introduce a new difficulty level called *ultimate*, with more, longer contours (see **Fig. 3[center right]** for an example, and the supplementary for more details). MAM again exhibits strong generalization capacity: a MAM trained on 1K *easy* images already achieves over 91% accuracy on *ultimate*, and MAMs trained with 5K images on any level achieve over 97% accuracy on *ultimate*. In contrast, an H-CNN trained on 900K *ultimate* images for $4\times$ longer than (Kim et al. 2020) only achieves less than 80% accuracy on *ultimate*.

cABC challenge

Task The cABC challenge (Kim et al. 2020) uses a pair of noisy, distorted letters as objects (**Fig 4[center]**), and seeks to identify whether two markers are on the same object. It complements the pathfinder challenge in that Gestalt strategies are expected to be ineffective, and it instead needs an object-specific recurrent routine that imposes high-level expectations about the shapes and structures of the letters. We follow the setups in (Kim et al. 2020), and use the proposed TD-H-CNN, a SOTA RNN that models both top-down and lateral interactions, as our baseline.

Elastic graphs and object-specific MAMs We model *elastic graphs* with object-specific MAMs, and match elastic graphs to noisy, distorted letters to solve the cABC challenge. An elastic graph is an undirected graph that models the letter as a composition of all the object parts represented by its vertices. Each vertex is associated with a reference location, and the object part it represents is allowed move around the reference location. An edge imposes an *elastic constraint* on the two connected object parts, by constraining their distance to be within a *perturb radius* of their reference distance. Elastic graphs use constrained elasticities to model deformations of letters without losing their shapes and structures. Several past works (Lades et al. 1993; Wiskott et al. 1997; George et al. 2017) have explored similar ideas. Our formulation and some efficient inference procedures are partly inspired by (George et al. 2017). We extract a set of elastic graphs from data (see **Learning**), and specify an object-specific MAM for each elastic graph. We merge all individual MAMs into a MAM \mathcal{M} , to model the presence of one training letter variation in one location on the image. We connect 2 copies $\mathcal{M}^{(1)}, \mathcal{M}^{(2)}$ of \mathcal{M} to the image with a sparsifier to model the presence of 2 noisy, distorted letters in each image.

Learning We can fully specify the object-specific MAM by extracting a set of elastic graphs from data. We achieve this by first sparsifying individual letters (available through ground truth segmentations) with the sparsifier, using a sin-

gle object part learned from 10 images (**Fig. 2[right]**). We define the vertices in the elastic graph using the sparse object parts activations from MPBP decoding, and heuristically identify a small number of elastic constraints to get the elastic graph (**Fig. 2[right]**).

Inference To make inference efficient, we again prune unlikely part variables and unnecessary attention variables by identifying rough locations of a set of best matching elastic graphs, and keep only their associated part and attention variables. We apply heuristic pairwise reasoning to approximate MPBP inference with the sparsifier. These procedures allow us to easily scale to models with 90K elastic graphs.

Results We follow (Kim et al. 2020) and experiment with 3 difficulty levels, *easy*, *medium*, *hard*. **Fig. 4[left]** shows the additional sample-efficiency of MAM compared to TD+H-CNN. TD+H-CNN completely fails with less than 20K training images, while MAM performs well above chance with only 50 training images. With 45K images, MAM performs worse than TD+H-CNN on *easy* and *medium*, but better on the more challenging and interesting *hard* level (see **Fig. 4[center]** for an example), and additionally gives interpretable and semantically meaningful elastic graphs matchings (**Fig. 4[right]**). **Tab. 2** shows MAM’s superior generalizability. TD+H-CNN trained on easier levels struggle to generalize to harder levels. TD+H-CNN trained on *hard* gives decent but lower performance on *easy* and *medium*. In contrast, MAMs trained on any level readily generalize to any other level, and generally exhibit consistent and sensible behavior of decreasing performance as difficulty increases.

Proof-of-concept using realistic images

Task We use realistic RGB-D images containing 39 different single objects in totes from the Object Segmentation Training Dataset (Zeng et al. 2017)¹. We randomly sample 70% of the data for training, and use the remaining 30% for testing. We use object masks to filter out images in which the objects are only partially visible. This results in 7797 training images and 5870 test images across all objects. We train object-specific MAMs to detect objects in test images.

Learning We obtain a dense set of edge detections for edges of 16 different orientations, and heuristically sparsify by picking detected edges within the object masks at roughly equal distances to construct elastic graphs.

Results We predict the object mask as the convex hull of object parts activations from MAM inference, and use the intersection over unions (IOUs) of the predicted object masks and the provided object masks as our performance measure. Note that the number of training images is just $1.3\times$ the number of test images, and objects in test images are in poses unseen in the training images. Despite challenges like deformable objects and adversarial surface properties, we are able to obtain a median IOU of 0.71 across all objects, demonstrating the sample-efficiency (small number of training images) and generalization capacities (generalizing to unseen novel poses) of the object-specific MAMs trained with rich prior information when applied to realistic images. See the supplementary for some visualizations.

¹Available at <https://vision.princeton.edu/projects/2016/apc/>

References

- Bader, S.; and Hitzler, P. 2005. Dimensions of neural-symbolic integration—a structured survey. *arXiv preprint cs/0511042*.
- Bahdanau, D.; Cho, K.; and Bengio, Y. 2014. Neural machine translation by jointly learning to align and translate. *arXiv preprint arXiv:1409.0473*.
- Boutillier, C.; Friedman, N.; Goldszmidt, M.; and Koller, D. 1996. Context-specific independence in Bayesian networks. In *Proceedings of the Twelfth international conference on Uncertainty in artificial intelligence*, 115–123.
- Bradbury, J.; Frostig, R.; Hawkins, P.; Johnson, M. J.; Leary, C.; Maclaurin, D.; Necula, G.; Paszke, A.; VanderPlas, J.; Wanderman-Milne, S.; and Zhang, Q. 2018. JAX: composable transformations of Python+NumPy programs.
- Chua, J.; and Felzenszwalb, P. F. 2020. Scene Grammars, Factor Graphs, and Belief Propagation. *J. ACM*, 67(4).
- Cohen, L.; and Zivan, R. 2017. Max-sum revisited: The real power of damping. In *International Conference on Autonomous Agents and Multiagent Systems*, 111–124. Springer.
- Fridman, A. 2003. Mixed markov models. *Proceedings of the National Academy of Sciences*, 100(14): 8092–8096.
- Friedman, N.; and Goldszmidt, M. 1998. Learning Bayesian networks with local structure. In *Learning in graphical models*, 421–459. Springer.
- Galassi, A.; Lippi, M.; and Torroni, P. 2020. Attention in natural language processing. *IEEE Transactions on Neural Networks and Learning Systems*.
- Garcez, A. d.; and Lamb, L. C. 2020. Neurosymbolic AI: The 3rd Wave. *arXiv preprint arXiv:2012.05876*.
- Garnelo, M.; and Shanahan, M. 2019. Reconciling deep learning with symbolic artificial intelligence: representing objects and relations. *Current Opinion in Behavioral Sciences*, 29: 17–23.
- George, D.; Lehrach, W.; Kansky, K.; Lázaro-Gredilla, M.; Laan, C.; Marthi, B.; Lou, X.; Meng, Z.; Liu, Y.; Wang, H.; et al. 2017. A generative vision model that trains with high data efficiency and breaks text-based CAPTCHAs. *Science*, 358(6368): eaag2612.
- Gilbert, C. D.; and Li, W. 2013. Top-down influences on visual processing. *Nat. Rev. Neurosci.*, 14(5): 350–363.
- Goyal, A.; Didolkar, A.; Ke, N. R.; Blundell, C.; Beaudoin, P.; Heess, N.; Mozer, M.; and Bengio, Y. 2021. Neural Production Systems. *arXiv:2103.01937*.
- Goyal, A.; Lamb, A.; Hoffmann, J.; Sodhani, S.; Levine, S.; Bengio, Y.; and Schölkopf, B. 2020. Recurrent Independent Mechanisms. In *International Conference on Learning Representations*.
- Han, K.; Wang, Y.; Chen, H.; Chen, X.; Guo, J.; Liu, Z.; Tang, Y.; Xiao, A.; Xu, C.; Xu, Y.; et al. 2020. A Survey on Visual Transformer. *arXiv preprint arXiv:2012.12556*.
- Harnad, S. 1990. The symbol grounding problem. *Physica D: Nonlinear Phenomena*, 42(1-3): 335–346.
- He, X.; and Yuille, A. 2010. Occlusion boundary detection using pseudo-depth. In *European Conference on Computer Vision*, 539–552. Springer.
- Hinton, G. E. 1990. Preface to the special issue on connectionist symbol processing. *Artificial Intelligence*, 46(1-2): 1–4.
- Hoiem, D.; Stein, A. N.; Efros, A. A.; and Hebert, M. 2007. Recovering occlusion boundaries from a single image. In *2007 IEEE 11th International Conference on Computer Vision*, 1–8. IEEE.
- Jin, Y.; and Geman, S. 2006. Context and Hierarchy in a Probabilistic Image Model. In *2006 IEEE Computer Society Conference on Computer Vision and Pattern Recognition (CVPR'06)*, volume 2, 2145–2152.
- Khan, S.; Naseer, M.; Hayat, M.; Zamir, S. W.; Khan, F. S.; and Shah, M. 2021. Transformers in Vision: A Survey. *arXiv preprint arXiv:2101.01169*.
- Kim, J.; Linsley, D.; Thakkar, K.; and Serre, T. 2020. Disentangling neural mechanisms for perceptual grouping. In *International Conference on Learning Representations*.
- Koller, D.; and Friedman, N. 2009. *Probabilistic graphical models: principles and techniques*. MIT press.
- Kschischang, F. R.; Frey, B. J.; and Loeliger, H.-A. 2001. Factor graphs and the sum-product algorithm. *IEEE Transactions on information theory*, 47(2): 498–519.
- Kubilius, J.; Schrimpf, M.; Kar, K.; Rajalingham, R.; Hong, H.; Majaj, N.; Issa, E.; Bashivan, P.; Prescott-Roy, J.; Schmidt, K.; Nayebi, A.; Bear, D.; Yamins, D. L.; and DiCarlo, J. J. 2019. Brain-Like Object Recognition with High-Performing Shallow Recurrent ANNs. In *Advances in Neural Information Processing Systems*, volume 32. Curran Associates, Inc.
- Lades, M.; Vorbruggen, J. C.; Buhmann, J.; Lange, J.; Von Der Malsburg, C.; Wurtz, R. P.; and Konen, W. 1993. Distortion invariant object recognition in the dynamic link architecture. *IEEE Transactions on computers*, 42(3): 300–311.
- Lake, B. M.; Salakhutdinov, R.; and Tenenbaum, J. B. 2015. Human-level concept learning through probabilistic program induction. *Science*, 350(6266): 1332–1338.
- Lamme, V. A.; Supèr, H.; and Spekreijse, H. 1998. Feed-forward, horizontal, and feedback processing in the visual cortex. *Curr. Opin. Neurobiol.*, 8(4): 529–535.
- Lee, J. B.; Rossi, R. A.; Kim, S.; Ahmed, N. K.; and Koh, E. 2019. Attention models in graphs: A survey. *ACM Transactions on Knowledge Discovery from Data (TKDD)*, 13(6): 1–25.
- Lee-Thorp, J.; Ainslie, J.; Eckstein, I.; and Ontanon, S. 2021. FNet: Mixing Tokens with Fourier Transforms. *arXiv preprint arXiv:2105.03824*.
- Liang, M.; and Hu, X. 2015. Recurrent convolutional neural network for object recognition. In *Proceedings of the IEEE conference on computer vision and pattern recognition*, 3367–3375.
- Liao, Q.; and Poggio, T. 2016. Bridging the gaps between residual learning, recurrent neural networks and visual cortex. *arXiv preprint arXiv:1604.03640*.

- Linsley, D.; Kim, J.; Veerabadrán, V.; Windolf, C.; and Serre, T. 2018. Learning long-range spatial dependencies with horizontal gated recurrent units. In *Advances in Neural Information Processing Systems*, 152–164.
- Marcus, G. 2018. Deep learning: A critical appraisal. *arXiv preprint arXiv:1801.00631*.
- Marcus, G. 2020. The next decade in AI: four steps towards robust artificial intelligence. *arXiv preprint arXiv:2002.06177*.
- Mittal, S.; Lamb, A.; Goyal, A.; Voleti, V.; Shanahan, M.; Lajoie, G.; Mozer, M.; and Bengio, Y. 2020. Learning to combine top-down and bottom-up signals in recurrent neural networks with attention over modules. In *International Conference on Machine Learning*, 6972–6986. PMLR.
- Mnih, V.; Heess, N.; Graves, A.; and Kavukcuoglu, K. 2014. Recurrent models of visual attention. *arXiv preprint arXiv:1406.6247*.
- Moskvichev, A.; and Liu, J. A. 2021. Updater-Extractor Architecture for Inductive World State Representations. *arXiv preprint arXiv:2104.05500*.
- Navigli, R. 2009. Word sense disambiguation: A survey. *ACM computing surveys (CSUR)*, 41(2): 1–69.
- Nayebi, A.; Bear, D.; Kubilius, J.; Kar, K.; Ganguli, S.; Sussillo, D.; DiCarlo, J. J.; and Yamins, D. L. 2018. Task-Driven Convolutional Recurrent Models of the Visual System. *Advances in Neural Information Processing Systems*, 31: 5290–5301.
- Nyman, H.; Pensar, J.; Koski, T.; and Corander, J. 2014. Stratified graphical models-context-specific independence in graphical models. *Bayesian Analysis*, 9(4): 883–908.
- Poole, D.; and Zhang, N. L. 2003. Exploiting contextual independence in probabilistic inference. *Journal of Artificial Intelligence Research*, 18: 263–313.
- Ren, X.; Fowlkes, C. C.; and Malik, J. 2005. Cue integration for figure/ground labeling. In *Proceedings of the 18th International Conference on Neural Information Processing Systems*, 1121–1128.
- Ren, X.; Fowlkes, C. C.; and Malik, J. 2006. Figure/ground assignment in natural images. In *European Conference on Computer Vision*, 614–627. Springer.
- Roelfsema, P. R. 2006. Cortical algorithms for perceptual grouping. *Annu. Rev. Neurosci.*, 29: 203–227.
- Roelfsema, P. R.; and Houtkamp, R. 2011. Incremental grouping of image elements in vision. *Attention, Perception, & Psychophysics*, 73(8): 2542–2572.
- Ronneberger, O.; Fischer, P.; and Brox, T. 2015. U-net: Convolutional networks for biomedical image segmentation. In *International Conference on Medical image computing and computer-assisted intervention*, 234–241. Springer.
- Serre, T. 2019. Deep learning: the good, the bad, and the ugly. *Annual review of vision science*, 5: 399–426.
- Shmulevich, I.; Dougherty, E. R.; Kim, S.; and Zhang, W. 2002. Probabilistic Boolean networks: a rule-based uncertainty model for gene regulatory networks. *Bioinformatics*, 18(2): 261–274.
- Silberman, N.; Shapira, L.; Gal, R.; and Kohli, P. 2014. A contour completion model for augmenting surface reconstructions. In *European Conference on Computer Vision*, 488–503. Springer.
- Spoerer, C. J.; McClure, P.; and Kriegeskorte, N. 2017. Recurrent convolutional neural networks: a better model of biological object recognition. *Frontiers in psychology*, 8: 1551.
- Sporns, O.; and Zwi, J. D. 2004. The small world of the cerebral cortex. *Neuroinformatics*, 2(2): 145–162.
- Sünderhauf, N.; Brock, O.; Scheirer, W.; Hadsell, R.; Fox, D.; Leitner, J.; Upcroft, B.; Abbeel, P.; Burgard, W.; Milford, M.; et al. 2018. The limits and potentials of deep learning for robotics. *The International Journal of Robotics Research*, 37(4-5): 405–420.
- Tay, Y.; Deghani, M.; Abnar, S.; Shen, Y.; Bahri, D.; Pham, P.; Rao, J.; Yang, L.; Ruder, S.; and Metzler, D. 2020. Long Range Arena: A Benchmark for Efficient Transformers. *arXiv preprint arXiv:2011.04006*.
- Vaswani, A.; Shazeer, N.; Parmar, N.; Uszkoreit, J.; Jones, L.; Gomez, A. N.; Kaiser, L.; and Polosukhin, I. 2017. Attention is all you need. *arXiv preprint arXiv:1706.03762*.
- Veličković, P.; Cucurull, G.; Casanova, A.; Romero, A.; Lio, P.; and Bengio, Y. 2017. Graph attention networks. *arXiv preprint arXiv:1710.10903*.
- Weiss, Y.; and Freeman, W. T. 2001. On the optimality of solutions of the max-product belief-propagation algorithm in arbitrary graphs. *IEEE Transactions on Information Theory*, 47(2): 736–744.
- Wellman, M. P.; and Henrion, M. 1993. Explaining ‘explaining away’. *IEEE Transactions on Pattern Analysis and Machine Intelligence*, 15(3): 287–292.
- Wiskott, L.; Krüger, N.; Kuiger, N.; and Von Der Malsburg, C. 1997. Face recognition by elastic bunch graph matching. *IEEE Transactions on pattern analysis and machine intelligence*, 19(7): 775–779.
- Xiong, Y.; Zeng, Z.; Chakraborty, R.; Tan, M.; Fung, G.; Li, Y.; and Singh, V. 2021. Nystromformer: A Nystrom-based Algorithm for Approximating Self-Attention. *arXiv preprint arXiv:2102.03902*.
- Zamir, A. R.; Wu, T.-L.; Sun, L.; Shen, W. B.; Shi, B. E.; Malik, J.; and Savarese, S. 2017. Feedback networks. In *Proceedings of the IEEE conference on computer vision and pattern recognition*, 1308–1317.
- Zeng, A.; Yu, K.-T.; Song, S.; Suo, D.; Walker Jr, E.; Rodriguez, A.; and Xiao, J. 2017. Multi-view Self-supervised Deep Learning for 6D Pose Estimation in the Amazon Picking Challenge. In *Proceedings of the IEEE International Conference on Robotics and Automation*.
- Zhu, S.-C.; and Mumford, D. 2007. *A stochastic grammar of images*. Now Publishers Inc.

Supplement to “Graphical Models with Attention for Context-Specific Independence and an Application to Perceptual Grouping”

Table of contents

1	Applying MAMs to perceptual grouping	2
1.1	Formal description	2
1.2	An illustrative toy example	2
2	Symbol grounding with the sparsifier	4
2.1	Formal definition for the sparsifier	4
2.2	Illustrative example of sparsifying a line with the sparsifier	5
2.3	Learning object parts from binary images	6
3	MPBP updates for involved factors	6
3.1	MPBP updates for the HOFs in MAMs:	6
3.2	MPBP updates for the OR factors in the sparsifier:	7
4	Hardware used for experiments	7
5	Details for the pathfinder challenge	7
5.1	Dataset details	7
5.2	Model	7
5.3	Pathfinder sparsification example	8
5.4	Learning	8
5.5	Pathfinder ultimate	9
6	Details for the cABC challenge	9
6.1	Dataset details	9
6.2	Model	9
6.3	Formal definitions of the object-specific MAM	9
6.4	cABC sparsification example	11
6.5	Learning elastic graphs for cABC	11
6.6	Efficient inference with the object-specific MAM	11

7	Details for experiments on realistic images	13
7.1	Dataset	13
7.2	Edge detection and heuristic sparsification	15
7.3	Visualization of results	15

1 Applying MAMs to perceptual grouping

1.1 Formal description

Our MAMs for perceptual grouping are binary higher-order MRFs containing two different types of variables: (1) binary part variables representing the presence/absence of object parts, and (2) binary attention variables representing the presence/absence of object parts interactions. Each part variable is associated with one HOF, connecting the part variable and its associated attention variables.

Use $|\cdot|$ to denote the cardinality of a set, $\mathcal{P}(\cdot)$ to denote all subsets of a set, and $\mathcal{P}_2(\cdot)$ to denote all cardinality 2 subsets of a set. We can specify our MAM's variables via the interaction graph, which is an undirected graph $\mathcal{G}_I = (\mathcal{V}_I, \mathcal{E}_I)$ where \mathcal{V}_I represents the set of vertices, and $\mathcal{E}_I = \{\{u, v\} : u, v \in \mathcal{V}_I, \exists \text{ an edge in } \mathcal{G}_I \text{ connecting } u, v\}$ represents the set of edges. To build a MAM from \mathcal{G}_I , we associate a binary part variable x_v with each vertex $v \in \mathcal{V}_I$, and a binary attention variable with each edge in \mathcal{E}_I . For ease of presentation, in what follows we represent the attention variable associated with $\{u, v\} \in \mathcal{E}_I$ interchangeably as either $a_{\{u, v\}}$ or $a_{\{x_u, x_v\}}$.

Let $a_{\sim x_v} = \{a_{\{u, v\}} : \{u, v\} \in \mathcal{E}_I\}$ be the set of attention variables associated with the part variable $x_v, v \in \mathcal{V}_I$. The corresponding MAM is specified by $|\mathcal{V}_I|$ factors f_{x_v} , one for each part variable x_v operating on $|a_{\sim x_v}| + 1$ variables (namely $\{x_v\} \cup a_{\sim x_v}$). Since all variables are binary, we represent a configuration for f_{x_v} by its entries that are ON, which is an element of $\mathcal{P}(\{x_v\} \cup a_{\sim x_v})$.

The HOF f_{x_v} is specified by a partition of $a_{\sim x_v}$ into M_{x_v} disjoint subsets of attention variables $a_{\sim x_v}^{(k)}, k = 1, \dots, M_{x_v}$. Intuitively, we can think of each $a_{\sim x_v}^{(k)}$ as an *interaction group*, consisting of a set of interchangeable interactions. The HOF f_{x_v} uses a set of prototypical interaction patterns to control x_v 's interaction with other part variables. Each prototypical interaction pattern turns on a set of interaction groups, and the HOF f_{x_v} makes context-specific decisions on which concrete interaction to use within each interaction group. In particular, this implies that for any valid configuration of the HOF f_{x_v} , at most one of the binary variables in each subset $a_{\sim x_v}^{(k)}$ can be ON. See Sec. 1.2 and **Fig. 1** for a toy example and its HOFs to illustrate the formal descriptions here.

Formally, we specify the HOF f_{x_v} with a set of M_{x_v} -dimensional binary vectors $\mathcal{B}_{x_v} \subset \{0, 1\}^{M_{x_v}}$ where $\mathbf{0} = (0, \dots, 0) \in \mathcal{B}_{x_v}$, and a potential in log domain $\mathcal{U}_{x_v} : \mathcal{B}_{x_v} \mapsto \mathbb{R}$. Here \mathcal{B}_{x_v} encodes the set of prototypical interaction patterns for f_{x_v} . Using $\mathbb{1}$ to denote the indicator function, each $\mathbf{b} = (b_1, \dots, b_{M_{x_v}}) \in \mathcal{B}_{x_v}$ induces a subset of valid configurations $\mathcal{C}_{x_v}(\mathbf{b})$ for the HOF f_{x_v} as

$$\mathcal{C}_{x_v}(\mathbf{b}) = \left\{ \mathbf{c} \in \mathcal{P}(\{x_v\} \cup a_{\sim x_v}) : \left| \mathbf{c} \cap a_{\sim x_v}^{(k)} \right| = b_k, k = 1, \dots, M_{x_v} \text{ and } \mathbb{1}_{x_v \in \mathbf{c}} = \mathbb{1}_{\|\mathbf{b}\|_1 > 0} \right\},$$

Each $\mathbf{c} \in \mathcal{C}_{x_v}(\mathbf{b})$ fully specifies a joint configuration of the part variable x_v and of all the attention variables $a_{\sim x_v}$. In particular, note that if the part variable x_v is ON, then at least one attention variable in $a_{\sim x_v}$ is ON. Reciprocally, if all the attention variables in $a_{\sim x_v}$ are OFF, then $\mathbf{b} = \mathbf{0}$ and the part variable x_v is OFF, meaning x_v does not interact with and has no effects on other part variables.

With a slight abuse of notation, for a configuration $\mathbf{c} \in \mathcal{P}(\{x_v\} \cup a_{\sim x_v})$, we use $f_{x_v}(\mathbf{c})$ to denote the potential in log domain of \mathbf{c} for f_{x_v} . The HOF f_{x_v} adopts a simple structure, and is defined as

$$f_{x_v}(\mathbf{c}) = \begin{cases} \mathcal{U}_{x_v} \left(\left(\left| \mathbf{c} \cap a_{\sim x_v}^{(1)} \right|, \dots, \left| \mathbf{c} \cap a_{\sim x_v}^{(M_{x_v})} \right| \right) \right), & \forall \mathbf{c} \in \bigcup_{\mathbf{b} \in \mathcal{B}_{x_v}} \mathcal{C}_{x_v}(\mathbf{b}) \\ -\infty, & \forall \mathbf{c} \notin \bigcup_{\mathbf{b} \in \mathcal{B}_{x_v}} \mathcal{C}_{x_v}(\mathbf{b}) \end{cases}$$

1.2 An illustrative toy example

Our MAMs for perceptual grouping provide a unified framework for symbolic recurrent computations. They coordinately model top-down parent/children interactions and lateral contextual object parts

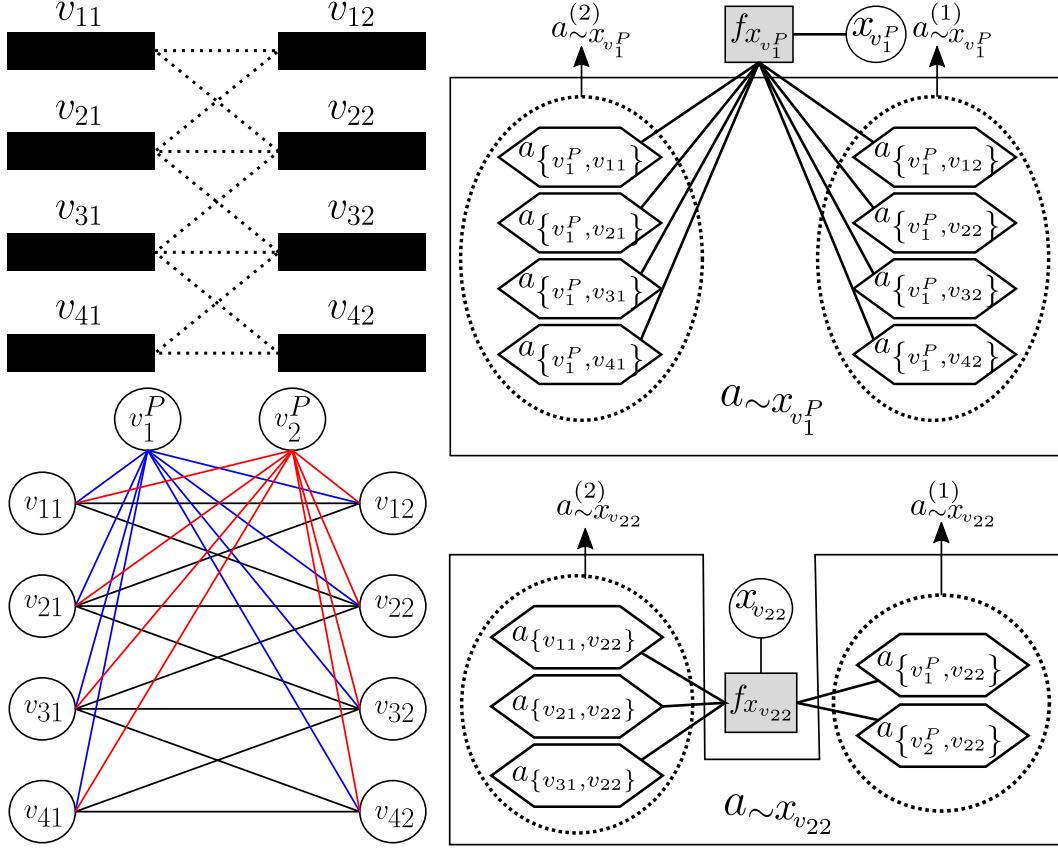


Figure 1: [Upper left] Toy example setup: line segments (solid black rectangles) and their potential continuations (dotted lines). [Lower left] The interaction graph for the corresponding MAM. [Upper right] The HOF $f_{x_{v_1^P}}$ modeling top-down interactions. [Lower right] The HOF $f_{x_{v_{22}}}$ coordinating top-down and lateral interactions.

interactions. They are formulated as binary higher-order MRFs, but differ from typical MRFs: MRFs commonly model graph vertices as variables and use graph edges to encode conditional independence, while MAMs model both graph vertices and edges as variables. The attention variables provide a convenient attention mechanism. They allow part variables to selectively pay attention to a small subset of other part variables while ignoring the rest, and enable efficient recurrent computations. In what follows, we work through a toy example to illustrate MAMs' coordinated modeling of both top-down and lateral interactions for perceptual grouping, as well as the efficiency gains from the attention mechanism through attention variables when compared with typical MRFs.

Consider a 4×2 grid of variables v_{ij} , $i = 1, \dots, 4$, $j = 1, 2$. Each variable represents a horizontal line segment that can continue, either in the horizontal direction or right above/below the horizontal direction, to form a line consisting of two segments. See **Fig. 1**[upper left] for an illustration. We further impose the global constraint that there can be at most two such lines.

We can easily specify a MAM to model the above. In addition to the 8 binary part variables $x_{v_{ij}}$, $i = 1, \dots, 4$, $j = 1, 2$, we introduce 2 additional variables v_1^P, v_2^P and their associated part variables $x_{v_1^P}, x_{v_2^P}$, representing possible presence of at most 2 lines. We specify the interaction graph in **Fig. 1**[lower left], and the complete factor graph in **Fig. 2**. This MAM contains 16 top-down attention variables $a_{\{v_\ell^P, v_{ij}\}}$, $\ell = 1, 2$, $i = 1, \dots, 4$, $j = 1, 2$, and 10 lateral attention variables $a_{\{v_{i_1}, v_{i_2}\}}$, $1 \leq i_1, i_2 \leq 4$, $|i_1 - i_2| \leq 1$. We use the HOF $f_{x_{v_\ell^P}}$, $\ell = 1, 2$ (**Fig. 1**[upper right]) to capture the possible presence of line $x_{v_\ell^P}$ and its top-down interaction with exactly 2 line segments by

$$a_{\sim x_{v_\ell^P}}^{(k)} = \left\{ a_{\{v_\ell^P, v_{ik}\}}, i = 1, \dots, 4 \right\} \quad \forall k = 1, 2; \quad \mathcal{B}_{x_{v_\ell^P}} = \{(0, 0), (1, 1)\}; \quad \mathcal{U}_{x_{v_\ell^P}}(\mathbf{b}) = 0, \quad \forall \mathbf{b} \in \mathcal{B}_{x_{v_\ell^P}}$$

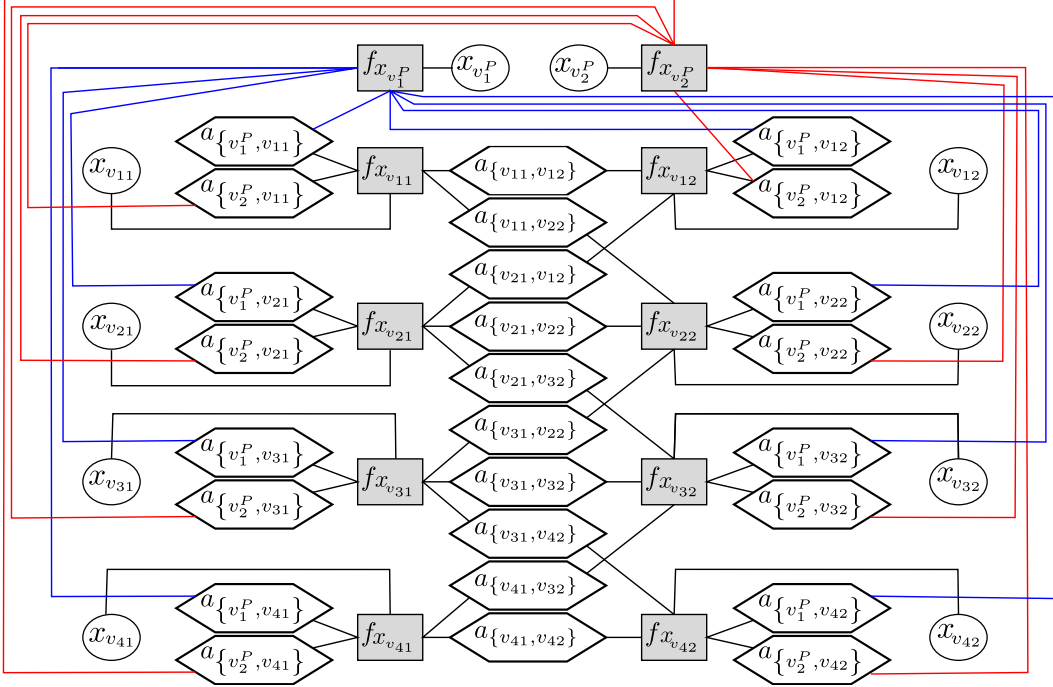


Figure 2: Factor graph for the MAM used in the toy example in Sec. 3.1 in the main text. Circles represent part variables. Hexagons represent attention variables. Shaded squares represent HOFs.

This guarantees that a line, if present, has to interact with exactly one line segment in each column. $\forall i = 1, \dots, 4, j = 1, 2$, we use the HOF $f_{x_{v_{ij}}}$ (**Fig. 1 [lower right]**) to capture the possible presence of line segment v_{ij} , its top-down interaction with one line and its lateral interaction with one of its continuation candidates by specifying $\mathcal{B}_{x_{v_{ij}}} = \{(0, 0), (1, 1)\}$, $\mathcal{U}_{x_{v_{ij}}}(\mathbf{b}) = 0, \forall \mathbf{b} \in \mathcal{B}_{x_{v_{ij}}}$ and

$$a_{\sim x_{v_{ij}}}^{(1)} = \{a_{\{v_\ell^P, v_{ij}\}}, \ell = 1, 2\}; \quad a_{\sim x_{v_{ij}}}^{(2)} = \{a_{\{v_{ij}, v_{\tilde{i}j}\}}, |\tilde{i} - i| \leq 1, \tilde{j} = 3 - j\}$$

The above MAM specifies a uniform distribution on all configurations with at most 2 lines, and coordinately models top-down and lateral interactions between part variables. Top-down interactions model the composition of a line with 2 line segments, and inform lateral interactions to enforce the global constraint of having at most 2 lines. However, they cannot prevent broken lines. Lateral interactions resolve ambiguities in top-down interactions, and ensure proper line segments continuations, which can be read off by looking at the attention variables, even if the line segments themselves are ambiguous about what the continuations are.

In contrast, an MRF operating only on binary part variables cannot do better than explicitly encoding all valid joint configurations in a single HOF. This is because of a complete lack of conditional independence relationships in the absence of attention variables. As an example, consider the pair of variables v_{12} and v_{41} : if $v_{11}, v_{22}, v_{31}, v_{42}$ are OFF, and v_{21}, v_{32} are ON, then v_{12} and v_{41} have to be both ON or both OFF. This implies v_{12} and v_{41} are not conditionally independent given all other variables. In fact, we can use the same argument to establish that, if we do not introduce attention variables, we do not have any pair of part variables that are conditionally independent given the rest.

2 Symbol grounding with the sparsifier

2.1 Formal definition for the sparsifier

A sparsifier is a binary higher-order MRF containing two different types of variables: (1) binary part variables, which are the same as the part variables in MAMs and represent the presence/absence of object parts, and (2) binary pixel variables, which represent pixels in a binary image. In this context, we describe the object part associated with a part variable by a set of pixels on the image, and consider

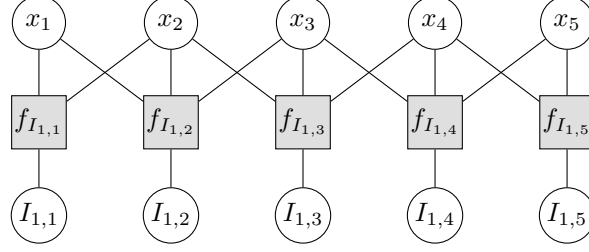


Figure 3: Factor graph for the toy example of sparsifying a line with the sparsifier in Sec. 2.2, with $K = 2$. The OR factor $f_{I_{1,j}}$ operates on the variables $\{I_{1,j}\} \cup \{x_k : 1 \leq k \leq 3K - 1 \text{ and } |j - k| \leq 1\}$. Each part variable x_j is associated with a unary potential that encourages it to be OFF.

the object part as a *parent* of its covered pixels. There is one OR factor per pixel variable, which is a HOF that connects the pixel variable and all its parent part variables.

Formally, for a given $M \times N$ binary image, we have MN pixel variables I_{ij} , $1 \leq i \leq M$, $1 \leq j \leq N$ and a set of part variables \mathcal{V}_S in the sparsifier. For a given part variable $x \in \mathcal{V}_S$, we use $I(x) \subset \{(i, j) : 1 \leq i \leq M, 1 \leq j \leq N\}$ to represent its associated object part. Let $x_{\sim I_{ij}} = \{x \in \mathcal{V}_S : (i, j) \in I(x)\}$ be the set of parent part variables for I_{ij} . The OR factor $f_{I_{ij}}$ associated with I_{ij} operates on $|x_{\sim I_{ij}}| + 1$ variables $\{I_{ij}\} \cup x_{\sim I_{ij}}$. We represent a configuration for $f_{I_{ij}}$ by its set of entries that are ON, which is an element of $\mathcal{P}(\{I_{ij}\} \cup x_{\sim I_{ij}})$. Using $f_{I_{ij}}(c)$ to denote the potential in log domain of configuration $c \in \mathcal{P}(\{I_{ij}\} \cup x_{\sim I_{ij}})$, the OR factor $f_{I_{ij}}$ is defined as

$$f_{I_{ij}}(c) = \begin{cases} 0, & \text{if } |x_{\sim I_{ij}} \cap c| > 0 \text{ and } I_{ij} \in c & \text{(at least one parent ON, pixel ON)} \\ 0, & \text{if } |c| = 0 & \text{(all parents OFF, pixel OFF)} \\ \log \pi_{01}, & \text{if } |x_{\sim I_{ij}} \cap c| > 0 \text{ and } I_{ij} \notin c & \text{(at least one parent ON, pixel OFF)} \\ \log \pi_{10}, & \text{if } |x_{\sim I_{ij}} \cap c| = 0 \text{ and } I_{ij} \in c & \text{(all parents OFF, pixel ON)} \end{cases}$$

where $0 \leq \pi_{01}, \pi_{10} < 0.5$ and $\log 0$ is assumed to represent $-\infty$.

2.2 Illustrative example of sparsifying a line with the sparsifier

We present herein a simple example to illustrate the *explaining away* type of reasoning implemented by the sparsifier, and discuss how it can be used to sparsify a binary image. Consider a $1 \times (3K - 1)$ binary image where all pixels are ON, i.e. a line of length $3K - 1$. We introduce a set of part variables x_1, \dots, x_{3K-1} , and define their corresponding object parts to be $I(x_j) = \{(1, k) : 1 \leq k \leq 3K - 1 \text{ and } |j - k| \leq 1\}$, i.e. short line segments consisting of two or three pixels. This implies that $x_{\sim I_{1j}} = \{x_k : 1 \leq k \leq 3K - 1 \text{ and } |j - k| \leq 1\}$, $1 \leq j \leq 3K - 1$, which are sets of size two or three. The OR factor $f_{I_{1j}}$ associated with I_{1j} operates on the $|x_{\sim I_{1j}}| + 1$ variables $\{I_{1j}\} \cup x_{\sim I_{1j}}$. See **Fig. 3** for the complete factor graph in the case $K = 2$.

We associate a unary potential in the log domain of 0 for being OFF and $\log \pi$ for being ON with each part variable, and set $0 < \pi_{10} < \pi < 1$. Under this setup, all the optimal joint configurations have exactly K part variables being ON, and each such joint configuration corresponds to a sparse representation of the line. In the case $K = 2$ shown in **Fig. 3**, these optimal joint configurations are $\{x_1, x_4\}$, $\{x_2, x_4\}$ and $\{x_2, x_5\}$:

1. If all the part variables are OFF, the potential of the joint configuration is $5 \log \pi_{10}$.
2. If one part variable is ON, the potential of the joint configuration is $\log \pi + 2 \log \pi_{10}$ (when x_2, x_3 , or x_4 is ON) or $\log \pi + 3 \log \pi_{10}$ (when x_1 or x_5 is ON),
3. The three joint configurations $\{x_1, x_4\}$, $\{x_2, x_4\}$ and $\{x_2, x_5\}$ all have potential $2 \log \pi$.
4. If more than three part variables are ON the joint potential is at most $3 \log \pi$.

Since $0 < \pi_{10} < \pi < 1$, we establish the optimality of $\{x_1, x_4\}$, $\{x_2, x_4\}$ and $\{x_2, x_5\}$.

2.3 Learning object parts from binary images

We use a special case of hierarchical compositional network (HCN) [1], where we have a single layer of latent variables and no POOL factors, to learn object parts directly from binary images. Intuitively, this is equivalent to replacing the predefined object parts by a set of binary weight variables covering a regular region (e.g. a rectangular region) in the sparsifier, and do MPBP inference jointly on the part, pixel and weight variables. Using the inference results from MPBP, we decode a set of ON weight variables which we use to define our learned object parts. The weight variables are shared convolutionally and across multiple images, allowing us to aggregate information from all images in the learning process and learn a small number of meaningful, generic and reusable object parts.

3 MPBP updates for involved factors

Due to the simple structures in the HOFs in MAMs and the OR factors in the sparsifier, MPBP updates for these factors can be done efficiently.

Use $\mathbb{M}^{u \rightarrow v} \in \mathbb{R}^2$ to denote the message (in log domain) from u to v , where u, v correspond to a pair of factor and variable. Since we can arbitrarily normalize the messages, for convenience and efficiency, in our implementations we use $m_{u \rightarrow v} = \mathbb{M}_2^{u \rightarrow v} - \mathbb{M}_1^{u \rightarrow v}$ as our messages (i.e. we normalize the messages by subtracting $\mathbb{M}_1^{u \rightarrow v}$ so that $\mathbb{M}_1^{u \rightarrow v}$ is always assumed to be 0).

3.1 MPBP updates for the HOFs in MAMs:

Due to the simple structure of the HOFs in MAMs, MPBP updates can be done efficiently. For the HOF f_{x_v} in a MAM, given the messages $m_{x_v \rightarrow f_{x_v}}, m_{a \rightarrow f_{x_v}}, a \in a_{\sim x_v}$ from variables to $f_{x_v}, \forall k = 1, \dots, M_{x_v}$, define

$$m_1^{(k)} = \max_{a \in a_{\sim x_v}^{(k)}} m_{a \rightarrow f_{x_v}}, \quad a^{(k)} = \operatorname{argmax}_{a \in a_{\sim x_v}^{(k)}} m_{a \rightarrow f_{x_v}}$$

$$m_2^{(k)} = \begin{cases} \max_{a \in a_{\sim x_v}^{(k)}: a \neq a^{(k)}} m_{a \rightarrow f_{x_v}} & \text{if } |a_{\sim x_v}^{(k)}| > 1 \\ 0 & \text{if } |a_{\sim x_v}^{(k)}| = 1, \end{cases}$$

so that $m_1^{(k)}$ denotes the largest message coming from all the elements in the set $a^{(k)}$ and $m_2^{(k)}$ denote the second largest message.

For a pair of factor f and variable v , the MPBP updates $m_{f \rightarrow v}$ are given by $\mathbb{M}_2^{f \rightarrow v} - \mathbb{M}_1^{f \rightarrow v}$, where

$$\mathbb{M}_2^{f_{x_v} \rightarrow x_v} = \max_{b \in \mathcal{B}_{x_v}, \|\mathbf{b}\|_1 > 0} \left[\mathcal{U}_{x_v}(\mathbf{b}) + m_{x_v \rightarrow f_{x_v}} + \sum_{k=1}^{M_{x_v}} b_k m_1^{(k)} \right]$$

$$\mathbb{M}_1^{f_{x_v} \rightarrow x_v} = \mathcal{U}_{x_v}((0, \dots, 0))$$

$$\mathbb{M}_2^{f_{x_v} \rightarrow a} = \max_{b \in \mathcal{B}_{x_v}: b_k = 1} \left[\mathcal{U}_{x_v}(\mathbf{b}) + m_{x_v \rightarrow f_{x_v}} + \sum_{\ell \neq k} b_\ell m_1^{(\ell)} \right], \quad a \in a_{\sim x_v}^{(k)}, \quad a \neq a^{(k)}$$

$$\mathbb{M}_1^{f_{x_v} \rightarrow a} = \max_{b \in \mathcal{B}_{x_v}} \left[\mathcal{U}_{x_v}(\mathbf{b}) + \mathbb{1}_{\|\mathbf{b}\|_1 > 0} m_{x_v \rightarrow f_{x_v}} + \sum_{\ell=1}^{M_{x_v}} b_\ell m_1^{(\ell)} \right], \quad a \in a_{\sim x_v}^{(k)}, \quad a \neq a^{(k)}$$

$$\mathbb{M}_2^{f_{x_v} \rightarrow a^{(k)}} = \max_{b \in \mathcal{B}_{x_v}: b_k = 1} \left[\mathcal{U}_{x_v}(\mathbf{b}) + m_{x_v \rightarrow f_{x_v}} + \sum_{\ell \neq k} b_\ell m_1^{(\ell)} \right]$$

$$\mathbb{M}_1^{f_{x_v} \rightarrow a^{(k)}} = \max_{b \in \mathcal{B}_{x_v}} \left[\mathcal{U}_{x_v}(\mathbf{b}) + \mathbb{1}_{\|\mathbf{b}\|_1 > 0} m_{x_v \rightarrow f_{x_v}} + \sum_{\ell \neq k} b_\ell m_1^{(\ell)} + b_k m_2^{(k)} \right]$$

3.2 MPBP updates for the OR factors in the sparsifier:

For a OR factor $f_{I_{ij}}$ in the sparsifier, if $|x_{\sim I_{ij}}| = 1$, the updates are trivial. If $|x_{\sim I_{ij}}| > 1$, given the messages $m_{I_{ij} \rightarrow f_{I_{ij}}}, m_{x \rightarrow f_{I_{ij}}}, x \in x_{\sim I_{ij}}$, define $x_1^{(ij)} = \operatorname{argmax}_{x \in x_{\sim I_{ij}}} m_{x \rightarrow f_{I_{ij}}}, x_2^{(ij)} = \operatorname{argmax}_{x \in x_{\sim I_{ij}}, x \neq x_1^{(ij)}} m_{x \rightarrow f_{I_{ij}}}$.

Use m^+ to denote $\max\{0, m\}$, and $m \vee n$ to denote $\max\{m, n\}$. For a pair of factor f and variable v , the MPBP updates $m_{f \rightarrow v}$ are given by $\mathbb{M}_2^{f \rightarrow v} - \mathbb{M}_1^{f \rightarrow v}$, where

$$\begin{aligned} \mathbb{M}_2^{f_{I_{ij}} \rightarrow I_{ij}} &= \left[m_{x^{(ij)} \rightarrow f_{I_{ij}}} + \sum_{x \neq x^{(ij)}} m_{x \rightarrow f_{I_{ij}}}^+ \right] \vee \log \pi_{10} \\ \mathbb{M}_1^{f_{I_{ij}} \rightarrow I_{ij}} &= \left(\log \pi_{01} + m_{x^{(ij)} \rightarrow f_{I_{ij}}} + \sum_{x \neq x^{(ij)}} m_{x \rightarrow f_{I_{ij}}}^+ \right)^+ \\ \mathbb{M}_2^{f_{I_{ij}} \rightarrow x_1^{(ij)}} &= m_{I_{ij} \rightarrow f_{I_{ij}}} \vee \log \pi_{01} + \sum_{q \in x_{\sim I_{ij}}, q \neq x_1^{(ij)}} m_{q \rightarrow f_{I_{ij}}}^+ \\ \mathbb{M}_1^{f_{I_{ij}} \rightarrow x_1^{(ij)}} &= \left(m_{I_{ij} \rightarrow f_{I_{ij}}} + \log \pi_{10} \right)^+ \vee \left(m_{I_{ij} \rightarrow f_{I_{ij}}} \vee \log \pi_{01} + m_{x_2^{(ij)} \rightarrow f_{I_{ij}}} + \sum_{q \neq x_2^{(ij)}} m_{q \rightarrow f_{I_{ij}}}^+ \right) \end{aligned}$$

and $\forall x \neq x_1^{(ij)}$,

$$\begin{aligned} \mathbb{M}_2^{f_{I_{ij}} \rightarrow x} &= m_{I_{ij} \rightarrow f_{I_{ij}}} \vee \log \pi_{01} + \sum_{q \in x_{\sim I_{ij}}, q \neq x} m_{q \rightarrow f_{I_{ij}}}^+, \forall x \neq x_1^{(ij)} \\ \mathbb{M}_1^{f_{I_{ij}} \rightarrow x} &= \left(m_{I_{ij} \rightarrow f_{I_{ij}}} + \log \pi_{10} \right)^+ \vee \left(m_{I_{ij} \rightarrow f_{I_{ij}}} \vee \log \pi_{01} + m_{x_1^{(ij)} \rightarrow f_{I_{ij}}} + \sum_{q \in x_{\sim I_{ij}}, q \neq x, x_1^{(ij)}} m_{q \rightarrow f_{I_{ij}}}^+ \right) \end{aligned}$$

4 Hardware used for experiments

We use machines with 32 Intel Xeon E5-2620 CPUs and 2 GeForce RTX 2080 Ti GPUs for experiments.

5 Details for the pathfinder challenge

5.1 Dataset details

The *easy*, *medium* and *hard* pathfinder datasets used in our experiments were generated using code provided by the authors, available at <https://github.com/drewlinsley/pathfinder>. See **Fig. 4** for example images from the 3 difficulty levels.

The code was released under the MIT license.

5.2 Model

The MAM for the pathfinder challenges uses $T \times M \times N$ part variables $x_{trc}, 1 \leq t \leq T, 1 \leq r \leq M, 1 \leq c \leq N$ to represent the possible presence of T types of object parts in an $M \times N$ grid of locations. Let $\{(t_1, t_2, \Delta r, \Delta c), (t_2, t_1, -\Delta r, -\Delta c)\}, 1 \leq t_1, t_2 \leq T, \Delta r, \Delta c \in \mathbb{Z}$ denote the co-occurrence of 2 object parts of types t_1, t_2 , where the relative displacement of the type t_2 object part with respect to the type t_1 object part is $(\Delta r, \Delta c)$. Each co-occurrence

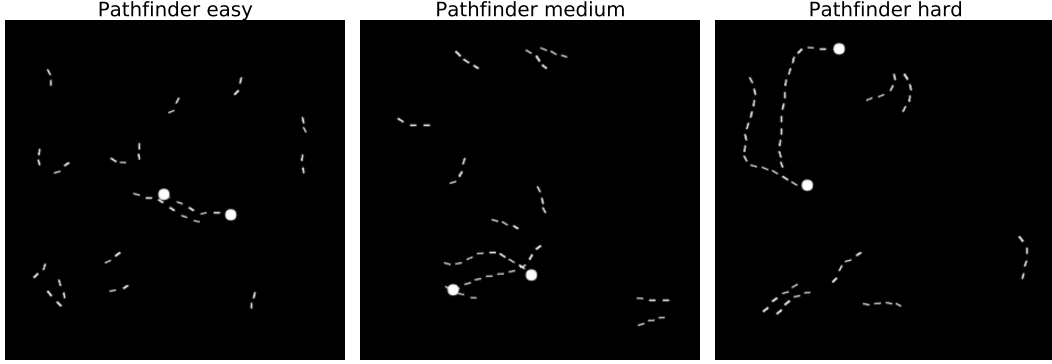


Figure 4: Pathfinder example images from the 3 difficulty levels (*easy*, *medium* and *hard*).

$\{(t_1, t_2, \Delta r, \Delta c), (t_2, t_1, -\Delta r, -\Delta c)\}$ is applied convolutionally and defines a set of attention variables $\left\{a_{\{x_{t_1 r_1 c_1}, x_{t_2 r_2 c_2}\}} : r_2 - r_1 = \Delta r, c_2 - c_1 = \Delta c, 1 \leq r_1, r_2 \leq M, 1 \leq c_1, c_2 \leq N\right\}$. The attention variables in the MAM are given by the union of the above sets of attention variables. We learn $T = 16$ types of object parts (**Fig. 5[left]**) from 10 training images, and extract co-occurrences of object parts from data. For x_{trc} , we partition its associated attention variables $a_{\sim x_{trc}}$ into 2 sets to capture possible contour continuations on both sides. The HOF $f_{x_{trc}}$ is specified by (1) the set of prototypical interaction patterns $\mathcal{B}_{x_{trc}} = \{(0, 0), (0, 1), (1, 0), (1, 1)\}$, which indicates that a contour should continue on one or both sides, and (2) the potential in log domain $\mathcal{U}_{x_{trc}}((0, 0)) = \mathcal{U}_{x_{trc}}((1, 1)) = 0, \mathcal{U}_{x_{trc}}((0, 1)) = \mathcal{U}_{x_{trc}}((1, 0)) = -1.6$, which penalizes contour termination and encourages the contour to be OFF or continue on both sides. We connect the MAM to the image with the sparsifier to model the presence of a variable number of broken contours.

5.3 Pathfinder sparsification example

See **Fig. 5** for an example of sparsifying pathfinder images.

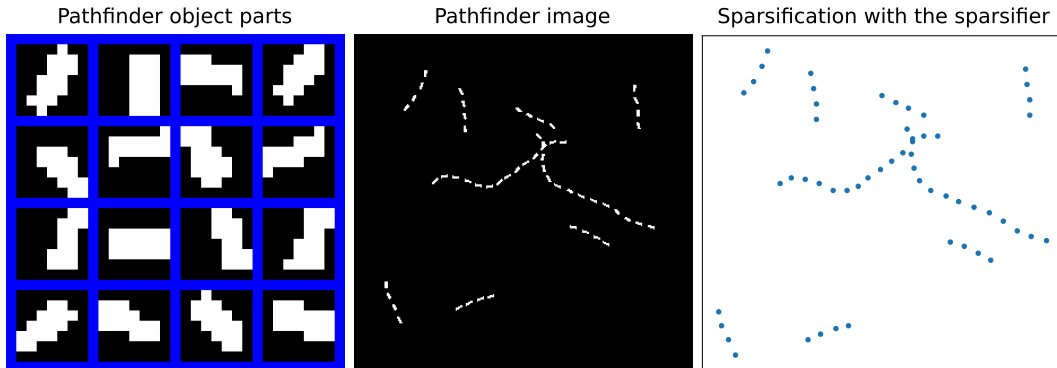


Figure 5: Sparsifying pathfinder images.

5.4 Learning

Learning: Learning of object parts and sparsifications are done with $\pi_{01} = 0.07, \pi_{10} = 0.0019$, and a unary potential in log domain of 0 for OFF and -20 for ON for all part variables to promote sparse object part activations. For sparsifications, we repeat MPBP 10 times for each individual contour to account for randomness. We define the MAM by aggregating co-occurrences from all individual contours while filtering out any co-occurrence whose relative frequency is less than 1.7×10^{-7} .

5.5 Pathfinder ultimate

In the original pathfinder datasets, for *easy*, there are two long contours of length 6, and 15 distractor contours of length 2 (**Fig. 4[left]**). For *medium*, there are two long contours of length 9, and 9 distractor contours of length 3 (**Fig. 4[center]**). For *hard*, there are two long contours of length 14, and 7 distractor contours of length 4 (**Fig. 4[right]**).

Since only the *hard* difficulty level proves to be challenging, we generate a new *ultimate* difficulty level by modifying the original data generation code to further probe the generalization capacities of MAM and H-CNN. For each *ultimate* image: (1) we first draw two long contours, each one with a length selected uniformly in $[20, 30]$; (2) we then draw two long distractors, each one with a length selected uniformly in $[15, 30]$ (3) we finally draw at most 8 short distractors with length selected uniformly in $[6, 14]$. See **Fig. 4[center right]** in the main text for an example.

6 Details for the cABC challenge

6.1 Dataset details

We use datasets provided by the authors at <https://openreview.net/forum?id=HJxrVA4FDS>, available for download at <https://bit.ly/2wdQYGd>. See **Fig. 4** for example images from the 3 difficulty levels.

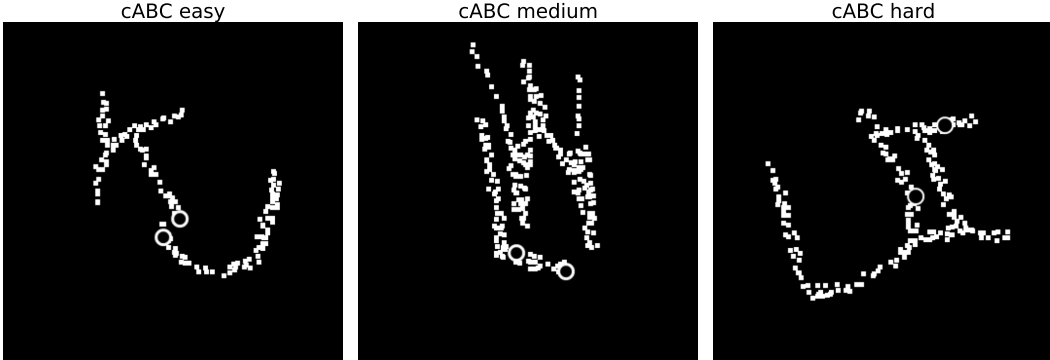


Figure 6: cABC example images from the 3 difficulty levels (*easy*, *medium* and *hard*).

6.2 Model

We model *elastic graphs* with object-specific MAMs, and match elastic graphs to noisy, distorted letters to solve the cABC challenge. An elastic graph $\mathcal{G}_E(\eta) = (\mathcal{V}_E, \mathcal{E}_E, \eta)$ is an undirected graph where \mathcal{V}_E represents its set of vertices and $\mathcal{E}_E = \{\{u, v\} : u, v \in \mathcal{V}_E, \exists \text{ an edge in } \mathcal{G}_E \text{ connecting } u, v\}$. Each $v \in \mathcal{V}_E$ represents an object part, and each $\{u, v\} \in \mathcal{E}_E$ represents an *elastic constraint* on u, v . An elastic graph models the letter as a composition of all the object parts represented by the vertices. We associate a reference location (r_v, c_v) with $v \in \mathcal{V}_E$, which indicates the expected location of the corresponding object part. We allow the vertex $v \in \mathcal{V}_E$ to move around, and use $(\tilde{r}_v, \tilde{c}_v)$ to denote its actual location. We use $\eta \geq 1$ to restrict the actual locations of the vertices to be $0 \leq \tilde{r}_v - r_v, \tilde{c}_v - c_v < \eta, \forall v \in \mathcal{V}_E$. We associate a *perturb radius* $\gamma_{\{u, v\}}$ with each edge $\{u, v\} \in \mathcal{E}_E$, which constrains the actual relative displacements $(\tilde{r}_v - \tilde{r}_u, \tilde{c}_v - \tilde{c}_u)$ to differ (in L_∞ norm) by no more than $\gamma_{\{u, v\}}$ from the reference relative displacements $(r_v - r_u, c_v - c_u)$, i.e. $|\tilde{r}_v - \tilde{r}_u - (r_v - r_u)| \leq \gamma_{\{u, v\}}, |\tilde{c}_v - \tilde{c}_u - (c_v - c_u)| \leq \gamma_{\{u, v\}}$.

6.3 Formal definitions of the object-specific MAM

Elastic graphs are inherently shift invariant, and are completely specified by the relative displacements of its vertices. For ease of presentation, we define $(r^{\mathcal{G}_E(\eta)}, c^{\mathcal{G}_E(\eta)}) = (\min_{v \in \mathcal{V}_E} r_v, \min_{v \in \mathcal{V}_E} c_v)$ as the *anchor point* of $\mathcal{G}_E(\eta)$ with reference locations $\{(r_v, c_v), v \in \mathcal{V}_E\}$. We can transform an elastic graph $\mathcal{G}_E(\eta)$ with anchor point $(r^{\mathcal{G}_E(\eta)}, c^{\mathcal{G}_E(\eta)})$ into an elastic graph $\bar{\mathcal{G}}_E(\eta)$ with anchor

point $(r^{\bar{\mathcal{G}}_E(\eta)}, c^{\bar{\mathcal{G}}_E(\eta)})$ by updating the reference location of vertex $v \in \mathcal{V}_E$ from (r_v, c_v) to $(r_v - r^{\mathcal{G}_E(\eta)} + r^{\bar{\mathcal{G}}_E(\eta)}, c_v - c^{\mathcal{G}_E(\eta)} + c^{\bar{\mathcal{G}}_E(\eta)})$.

We can specify an object-specific MAM for a given elastic graph $\mathcal{G}_E(\eta)$. We associate a part variable $x_{v\tilde{r}_v\tilde{c}_v}^{\mathcal{G}_E(\eta)}$ with each allowed location $(\tilde{r}_v, \tilde{c}_v), v \in \mathcal{V}_E, 0 \leq \tilde{r}_v - r_v, \tilde{c}_v - c_v < \eta$. For each edge $\{u, v\} \in \mathcal{E}_E$, we associate a lateral attention variable $a_{\{x_{u\tilde{r}_u\tilde{c}_u}^{\mathcal{G}_E(\eta)}, x_{v\tilde{r}_v\tilde{c}_v}^{\mathcal{G}_E(\eta)}\}}$ with each pair of locations $(\tilde{r}_u, \tilde{c}_u), (\tilde{r}_v, \tilde{c}_v)$ in an allowed relative displacement (i.e. $|(\tilde{r}_v - \tilde{r}_u) - (r_v - r_u)| \leq \gamma_{\{u,v\}}, |(\tilde{c}_v - \tilde{c}_u) - (c_v - c_u)| \leq \gamma_{\{u,v\}}$). We additionally introduce the part variable $x^{\mathcal{G}_E(\eta)}$ to represent the possible presence of the letter, and the top-down attention variables

$$a_{\{x^{\mathcal{G}_E(\eta)}, x_{v\tilde{r}_v\tilde{c}_v}^{\mathcal{G}_E(\eta)}\}}, v \in \mathcal{V}_E, 0 \leq \tilde{r}_v - r_v, \tilde{c}_v - c_v < \eta$$

For the HOF $f_{x^{\mathcal{G}_E(\eta)}}$, we partition $a_{\sim x^{\mathcal{G}_E(\eta)}}$ into $M_{x^{\mathcal{G}_E(\eta)}} = |\mathcal{V}_E|$ disjoint sets of attention variables

$$a_{\sim x^{\mathcal{G}_E(\eta)}}^{(k)} = \left\{ a_{\{x^{\mathcal{G}_E(\eta)}, x_{v_k\tilde{r}_{v_k}\tilde{c}_{v_k}}^{\mathcal{G}_E(\eta)}\}} : 0 \leq \tilde{r}_{v_k} - r_{v_k}, \tilde{c}_{v_k} - c_{v_k} < \eta \right\}, k = 1, \dots, |\mathcal{V}_E|$$

where $\mathcal{V}_E = \{v_1, \dots, v_{|\mathcal{V}_E|}\}$ is some ordering of all the vertices in \mathcal{V}_E . Define $\mathcal{B}_{x^{\mathcal{G}_E(\eta)}} = \{(0, \dots, 0), (1, \dots, 1)\}$ and $\mathcal{U}_{x^{\mathcal{G}_E(\eta)}}(b) = 0, \forall b \in \mathcal{B}_{x^{\mathcal{G}_E(\eta)}}$. Intuitively, this enforces that, if the letter is present, then each $v \in \mathcal{V}_E$ must be present, at exactly one of the allowed location.

For the HOFs $f_{x_{v\tilde{r}_v\tilde{c}_v}^{\mathcal{G}_E(\eta)}}, v \in \mathcal{V}_E, 0 \leq \tilde{r}_v - r_v, \tilde{c}_v - c_v < \eta$, we partition $a_{\sim x_{v\tilde{r}_v\tilde{c}_v}^{\mathcal{G}_E(\eta)}}$ into $M_v^{\mathcal{G}_E(\eta)} = |\{u \in \mathcal{V}_E : \{u, v\} \in \mathcal{E}_E\}| + 1$ disjoint sets of attention variables

$$a_{\sim x_{v\tilde{r}_v\tilde{c}_v}^{\mathcal{G}_E(\eta)}}^{(k)} = a_{\sim x_{v\tilde{r}_v\tilde{c}_v}^{\mathcal{G}_E(\eta)}} \cap a_{\sim x_{u_k\tilde{r}_{u_k}\tilde{c}_{u_k}}^{\mathcal{G}_E(\eta)}}, k = 1, \dots, M_v^{\mathcal{G}_E(\eta)} - 1, a_{\sim x_{v\tilde{r}_v\tilde{c}_v}^{\mathcal{G}_E(\eta)}}^{(M_v^{\mathcal{G}_E(\eta)})} = \left\{ a_{\{x^{\mathcal{G}_E(\eta)}, x_{v\tilde{r}_v\tilde{c}_v}^{\mathcal{G}_E(\eta)}\}} \right\}$$

where we impose some ordering $\{u \in \mathcal{V}_E : \{u, v\} \in \mathcal{E}_E\} = \{u_1, \dots, u_{M_v^{\mathcal{G}_E(\eta)} - 1}\}$. We define $\mathcal{B}_{x_{v\tilde{r}_v\tilde{c}_v}^{\mathcal{G}_E(\eta)}} = \{(0, \dots, 0), (1, \dots, 1)\}$ and $\mathcal{U}_{x_{v\tilde{r}_v\tilde{c}_v}^{\mathcal{G}_E(\eta)}}((0, \dots, 0)) = -1000, \mathcal{U}_{x_{v\tilde{r}_v\tilde{c}_v}^{\mathcal{G}_E(\eta)}}((1, \dots, 1)) = 0$.

For the cABC challenge, assume the sizes of the images imply that object parts can be instantiated on an $M \times M$ grid. We extract elastic graphs from N letters in the training images using the procedure outlined in Sec. 6.5, and transform them into a set of elastic graphs $\mathcal{G}_E^{(n)}(M) = (\mathcal{V}_E^{(n)}, \mathcal{E}_E^{(n)}, M), n = 1, \dots, N$ whose anchor points are all $(1, 1)$. We construct N MAMs $\mathcal{M}^{\mathcal{G}_E^{(n)}(M)}, n = 1, \dots, N$ as described above, and merge them into a single MAM \mathcal{M} with part variables that live within the $M \times M$ grid $x_{v\tilde{r}_v\tilde{c}_v}^{\mathcal{G}_E^{(n)}(M)}, v \in \mathcal{V}_E^{(n)}, r_v \leq \tilde{r}_v \leq M, c_v \leq \tilde{c}_v \leq M, n = 1, \dots, N$, the lateral attention variables $a_{\{x_{u\tilde{r}_u\tilde{c}_u}^{\mathcal{G}_E^{(n)}(M)}, x_{v\tilde{r}_v\tilde{c}_v}^{\mathcal{G}_E^{(n)}(M)}\}}$ where $\{u, v\} \in \mathcal{E}_E^{(n)}, |(\tilde{r}_v - \tilde{r}_u) - (r_v - r_u)| \leq \gamma_{\{u,v\}}, |(\tilde{c}_v - \tilde{c}_u) - (c_v - c_u)| \leq \gamma_{\{u,v\}}, r_v \leq \tilde{r}_v \leq M, c_v \leq \tilde{c}_v \leq M, n = 1, \dots, N$ and collapsing the part variables $x^{\mathcal{G}_E^{(n)}(M)}$ into a single part variable $x^{\mathcal{M}}$, with top-down attention variables

$$a_{\{x^{\mathcal{M}}, x_{v\tilde{r}_v\tilde{c}_v}^{\mathcal{G}_E^{(n)}(M)}\}}, r_v \leq \tilde{r}_v \leq M, c_v \leq \tilde{c}_v \leq M, n = 1, \dots, N$$

The HOFs $f_{x_{v\tilde{r}_v\tilde{c}_v}^{\mathcal{G}_E^{(n)}(M)}}, r_v \leq \tilde{r}_v \leq M, c_v \leq \tilde{c}_v \leq M, n = 1, \dots, N$ remain the same (with $x^{\mathcal{G}_E^{(n)}(M)}$ replaced by $x^{\mathcal{M}}$), while for the HOF $f_{x^{\mathcal{M}}}$, we now partition $a_{\sim x^{\mathcal{M}}}$ into $M_{x^{\mathcal{M}}} = \sum_{n=1}^N |\mathcal{V}_E^{(n)}|$ disjoint sets of attention variables: $\forall n = 1, \dots, N, k = 1, \dots, |\mathcal{V}_E^{(n)}|$,

$$a_{\sim x^{\mathcal{M}}}^{(\sum_{i=1}^{n-1} |\mathcal{V}_E^{(i)}| + k)} = \left\{ a_{\{x^{\mathcal{M}}, x_{v_k\tilde{r}_{v_k}\tilde{c}_{v_k}}^{\mathcal{G}_E^{(n)}(M)}\}} : r_v \leq \tilde{r}_v \leq M, c_v \leq \tilde{c}_v \leq M \right\}$$

and $\mathcal{B}_{x\mathcal{M}} = \{(0, \dots, 0)\} \cup \{b^{(n)}, n = 1, \dots, N\}$, where $\forall n \in \{1, \dots, N\}$,

$$b_j^{(n)} = \begin{cases} 1, & \text{if } \sum_{i=1}^{n-1} |\mathcal{V}_E^{(i)}| < j \leq \sum_{i=1}^n |\mathcal{V}_E^{(i)}| \\ 0, & \text{otherwise} \end{cases}$$

and

$$\mathcal{U}_{x\mathcal{M}}((0, \dots, 0)) = -1000, \mathcal{U}_{x\mathcal{M}}(b) = 0, \forall b \in \mathcal{B}_{x\mathcal{M}}, b \neq (0, \dots, 0)$$

Intuitively, each individual $\mathcal{M}^{\mathcal{G}_E^{(n)}(M)}$ encodes the presence of the n th letter at a certain location on the image, while \mathcal{M} merges the individual MAMs to encode the presence of exactly one letter at a certain location on the image. We connect 2 copies $\mathcal{M}^{(1)}, \mathcal{M}^{(2)}$ of \mathcal{M} to the image with the sparsifier to model the presence of 2 noisy, distorted letters in each image.

6.4 cABC sparsification example

See **Fig. 2[center right]** and **Fig. 2[right]** in the main text for an example of sparsifying a noisy, distorted cABC letter. The vertices in the elastic graph in **Fig. 2[right]** in the main text represent the sparse set of object part activations given by sparsifying the binary input image (**Fig. 2[center right]** in the main text) with the sparsifier using a single object part learned from 10 training images (lower left of **Fig. 2[right]** in the main text).

6.5 Learning elastic graphs for cABC

Learning of the single object part and sparsifications are done using $\pi_{01} = 0.45$, $\pi_{10} = 0.05$, and a unary potential in log domain of 0 for OFF and -20 for ON for all part variables to promote sparse object part activations. We define the vertices in the elastic graph using the sparse object part activations from MPBP decoding.

Given a sparse set of object part activations (\mathcal{V}_E), we use **Alg. 1** to construct an elastic graph. In our experiments, we used perturbation factor 7.0, tolerance 2.0 and max connection length 200. These hyper-parameters were derived by doing a parameter sweep over integers and measuring performance on a small validation set.

Intuitively, we use the perturbation factor to capture the notion that the relative displacement of a pair of far-away object parts can vary more than that of a pair of close-by object parts. For a pair of object parts $u, v \in \mathcal{V}_E$, using $d_{u,v}$ to denote their Euclidean distance, the associated perturb radius is roughly given by $d_{u,v}$ divided by the perturb factor. To implement the constrained elasticities, a naive approach is to add an elastic constraint for every pair of vertices. However, this would result in an overly dense elastic graph and makes subsequent inference inefficient. In **Alg. 1**, we use a heuristic algorithm to add a small number of elastic constraints. We start from vertices that are closest together, and progressively add elastic constraints. For a given pair of vertices, we skip adding their elastic constraint if the desired elastic constraint can already be enforced using existing elastic constraints (up to the specified tolerance). We adopt a final refining step to account for rounding errors. Refer to **Alg. 1** for more details. See **Fig. 2[right]** in the main text for an example elastic graph.

6.6 Efficient inference with the object-specific MAM

In our formulation, we use \mathcal{M} to model the presence of a particular training letter at a certain location on the image. In practice, only a small number of training letters at a small number of locations would fit a given image well. To make inference efficient, we use fast feedforward operations to identify the rough locations of a small number of training letters (in the form of a small number of elastic graphs with different anchor points and small η), and do MPBP inference only with the relevant part and attention variables. All the hyper-parameters used in this section are empirically set with a validation set consisting of 1000 *easy* cABC images. The same set of hyper-parameters are then applied to all 3 difficulty levels (*easy*, *medium* and *hard*) without change.

We follow notations in Sec. 3.2 in the main text and in Sec. 3. For a given $M \times M$ image, use $m_{I_{ij}}$ to denote the evidence coming from the image to the pixel variable I_{ij} , $1 \leq i, j \leq M$. For a given

Algorithm 1: Adding edges to elastic graphs

Input: Elastic graph vertices \mathcal{V}_E and the associated reference locations $(r_v, c_v), \forall v \in \mathcal{V}_E$, perturbation factor p , tolerance t , max connection length l

Output: Elastic graph edges \mathcal{E}_E and the associated perturb radius $\gamma_{\{u,v\}}, \forall \{u,v\} \in \mathcal{E}_E$

Procedure GetEdges($\mathcal{V}_E, r, c, p, t, l$)

```
 $C, d \leftarrow \text{GetPotentialEdges}(\mathcal{V}_E, r, c, l);$   
 $\mathcal{E}_E, \gamma \leftarrow \text{AddEdges}(C, d, p, t);$   
 $O \leftarrow \text{EdgeDepthFirstSearch}(\mathcal{E}_E, [], \text{AnyElementOf}(\mathcal{V}_E));$   
 $\gamma \leftarrow \text{RefineEdges}(O, d, \gamma, p);$   
return  $\mathcal{E}_E, \gamma;$ 
```

Procedure GetPotentialEdges(\mathcal{V}_E, r, c, l)

```
 $P \leftarrow []$   
for  $u$  in  $\mathcal{V}_E$  do  
  for  $v$  in  $\mathcal{V}_E$  do  
     $d_{u,v} \leftarrow \sqrt{(r_v - r_u)^2 + (c_v - c_u)^2}$   
    if  $d_{u,v} < l$  and  $\{u, v\} \notin P$  then  
       $P \leftarrow \text{append}(P, \{u, v\})$   
    end  
  end  
end  
 $C \leftarrow \text{sorted}(P)$  by  $d_{u,v}$  ascending  
return  $C, d;$ 
```

Procedure AddEdges(C, d, p, t)

```
 $\mathcal{E}_E \leftarrow \{\}$   
 $\gamma \leftarrow \{\}$   
for  $\{u, v\}$  in  $C$  do  
   $i \leftarrow \max\left\{1, \frac{d_{u,v}}{p}\right\}$   
   $n \leftarrow \text{ShortestPath}(u, v)$  in  $\mathcal{E}_E$  with edge weights  $\gamma$  // infinity if no path exists  
  if  $n > it$  then  
     $\mathcal{E}_E \leftarrow \mathcal{E}_E \cup \{\{u, v\}\}$   
     $\gamma_{\{u,v\}} \leftarrow \lceil i \rceil$   
  end  
end  
return  $\mathcal{E}_E, \gamma;$ 
```

Procedure EdgeDepthFirstSearch(\mathcal{E}_E, O, u)

```
for  $v \in \{v \in \mathcal{V}_E \mid \{u, v\} \in \mathcal{E}_E\}$  do  
  if  $\{u, v\} \notin O$  then  
     $O \leftarrow \text{append}(O, \{u, v\})$   
     $O \leftarrow \text{concatenate}(O, \text{EdgeDepthFirstSearch}(\mathcal{E}_E, O, v))$   
  end  
end  
return  $O;$ 
```

Procedure RefineEdges(O, d, γ, p)

```
 $\eta \leftarrow 0;$   
for  $\{u, v\}$  in  $O$  do  
   $i \leftarrow \max\left\{1, \frac{d_{u,v}}{p}\right\}$   
  if  $|\lceil i \rceil - i + \eta| < |\lfloor i \rfloor - i + \eta|$  then  
     $\gamma_{\{u,v\}} = \lceil i \rceil$   
     $\eta \leftarrow \lceil i \rceil - i + \eta$   
  else  
     $\gamma_{\{u,v\}} = \lfloor i \rfloor$   
     $\eta \leftarrow \lfloor i \rfloor - i + \eta$   
  end  
end  
return  $\gamma$ 
```

elastic graph $\mathcal{G}_E(\eta) = (\mathcal{V}_E, \mathcal{E}_E, \eta)$, we define its *score* to be

$$\frac{1}{|\mathcal{V}_E|^{0.76}} \left(\sum_{v \in \mathcal{V}_E} \max_{\tilde{r}_v, \tilde{c}_v: 0 \leq \tilde{r}_v - r_v, \tilde{c}_v - c_v < \eta} \sum_{(i,j) \in I(x_{v\tilde{r}_v\tilde{c}_v}^{\mathcal{G}_E(\eta)})} m_{I_{ij}} \right)$$

Intuitively, to get the score of an elastic graph $\mathcal{G}_E(\eta)$, for each object part $v \in \mathcal{V}_E$, we obtain the score of the object part at a given location $(\tilde{r}_v, \tilde{c}_v)$ by summing up the evidence from pixels that are part of this object part, i.e. $\sum_{(i,j) \in I(x_{v\tilde{r}_v\tilde{c}_v}^{\mathcal{G}_E(\eta)})} m_{I_{ij}}$. We maximize over all the allowed locations $0 \leq \tilde{r}_v - r_v, \tilde{c}_v - c_v < \eta$ of the object part $v \in \mathcal{V}_E$ to get the score of the object part $\max_{\tilde{r}_v, \tilde{c}_v: 0 \leq \tilde{r}_v - r_v, \tilde{c}_v - c_v < \eta} \sum_{(i,j) \in I(x_{v\tilde{r}_v\tilde{c}_v}^{\mathcal{G}_E(\eta)})} m_{I_{ij}}$, and we sum over all the object parts in the elastic graph to get the unnormalized score of the elastic graph $\sum_{v \in \mathcal{V}_E} \max_{\tilde{r}_v, \tilde{c}_v: 0 \leq \tilde{r}_v - r_v, \tilde{c}_v - c_v < \eta} \sum_{(i,j) \in I(x_{v\tilde{r}_v\tilde{c}_v}^{\mathcal{G}_E(\eta)})} m_{I_{ij}}$. We normalize the score by $\frac{1}{|\mathcal{V}_E|^{0.76}}$ to prevent the process from being dominated by elastic graphs with a large number of vertices.

In our experiments, we first downsample the original 350×350 images to 256×256 images (i.e. $M = 256$), and use circles of radius 4 as our only object part. We define $m_{ij} = 1.0$ for the pixel (i, j) that is ON, and $m_{ij} = -0.89$ for the pixel (i, j) that is OFF. To make the elastic graphs scores informative, instead of using $\eta = 256$ to allow the vertices to move around as much as possible, we use $\eta = 15$ to evaluate how well an elastic graph fits in a local region. To cover the entire image, we shift the anchor points from $(1, 1)$ to the right/downwards with a step size of 13, i.e. we consider the elastic graph $\mathcal{G}_E(15)$ and its transformed copies with anchor points $(1 + 13 \times k, 1 + 13 \times \ell)$, $k, \ell \in \mathbb{N}$. This implies that, for each elastic graph $\mathcal{G}_E(15)$, we are evaluating its scores at 400 different locations.

We evaluate the scores for all the elastic graphs and their transformed copies. For a given anchor point, we rank the elastic graphs with this anchor point based on their scores, and keep the top 3 elastic graph at each anchor point. We aggregate the top 3 elastic graphs from all 400 anchor points, and keep the top 140 (across all the anchor points) as estimates of the locations of the most promising elastic graphs.

We take the 140 most promising elastic graphs and use $\eta = 25$ to allow more invariance in the MAM inference. To parallelize the inference process, for each elastic graph $\mathcal{G}_E(25)$, we use $\sum_{(i,j) \in I(x_{v\tilde{r}_v\tilde{c}_v}^{\mathcal{G}_E(25)})} m_{I_{ij}}$ as the evidence for the part variable $x_{v\tilde{r}_v\tilde{c}_v}^{\mathcal{G}_E(25)}$, and do MPBP inference in parallel for all the elastic graphs. From the MPBP decodings, for each $v \in \mathcal{V}_E$, we can determine its most likely location, which we denote as (\hat{r}_v, \hat{c}_v) . We define $I(\mathcal{G}_E(25)) = \cup_{v \in \mathcal{V}_E} I(x_{v\hat{r}_v\hat{c}_v}^{\mathcal{G}_E(25)})$ as the set of pixels associated with the elastic graph MPBP decoding. For each pixel $(i, j) \in I(\mathcal{G}_E(25))$, use $\mathcal{N}((i, j), \mathcal{G}_E(25)) = \sum_{v \in \mathcal{V}_E} \mathbb{1}_{(i,j) \in I(x_{v\hat{r}_v\hat{c}_v}^{\mathcal{G}_E(25)})}$ to denote the number of object parts in the MPBP decoding that covers the pixel (i, j) .

As a final inference step, we approximate MPBP inference with the sparsifier with a heuristic pairwise reasoning step. More concretely, we consider all $\binom{140}{2} = 9730$ possible pairs of elastic graphs. We define the score of a given pair of elastic graphs $\mathcal{G}_E^{(1)}(25)$ and $\mathcal{G}_E^{(2)}(25)$ as

$$\sum_{(i,j) \in I(\mathcal{G}_E^{(1)}(25)) \cup I(\mathcal{G}_E^{(2)}(25))} \left[m_{I_{ij}} - \left(\mathcal{N}((i, j), \mathcal{G}_E^{(1)}(25)) + \mathcal{N}((i, j), \mathcal{G}_E^{(2)}(25)) - 1 \right) * 0.33 \right]$$

i.e. we sum up the evidence from all the involved pixels, while applying a small penalty for object parts that overlap with each other.

We pick the pair of elastic graphs with the highest score as our interpretation of the test image, and heuristically assign the two markers to classifier cABC test images.

7 Details for experiments on realistic images

7.1 Dataset

We use realistic RGB-D images containing 39 different single objects in totes from the Object Segmentation Training Dataset [2], available for download at <https://vision.princeton.edu/>



Figure 7: Visualization of MAM detections on realistic images for 6 objects (*barkely_hide_bones*, *clorox_utility_brush*, *cloud_b_plush_bear*, *fiskars_scissors_red*, *creativity_chenille_stems*, *oral_b_toothbrush_red*) from the Object Segmentation Training Dataset. Blue dots in the right column represent object part activations from MPBP inference with MAMs.

[projects/2016/apc/](#). For each object, we have multiple scenes. Each scene has the object in a different pose. For each scene, we have multiple frames. Each frame has the camera in a different pose. We use the RGB, depth and object masks associated with each frame as our train and test data. We randomly sample 70% of the scenes as training data, and use the remaining 30% as test data. Since we want to test an object-specific MAM modeling entire objects, we filter out frames in which the objects are only partially visible due to object and camera poses, by keeping frames with the largest mask sizes for each scene. For each training scene, we keep the top 3 frames. For each test scene, we keep the top 5 frames. This results in a dataset with 7797 training frames and 5870 test frames across all objects. See the left column in **Fig. 7** for the visualization of some example images.

7.2 Edge detection and heuristic sparsification

For edge detection, we take the maximum response from grayscale filters of 16 orientations over the 3 channels of RGB images, followed by a local suppression step similar to that used in Canny edge detection. See the middle column in **Fig. 7** for the visualization of the maximum response on test images from the detection of edges of 16 orientations.

For sparsification, we adopt a heuristic procedure, where we pick points roughly at equal distances. More concretely, we start from a random point, and greedily pick points at a distance close to our target distance, until we can no longer pick new points. From the set of unpicked points, we then randomly pick a new starting point that is at least the target distance away from already picked points, and continue the greedy procedure. We repeat until we can no longer find new points.

7.3 Visualization of results

See the right column in **Fig. 7** for the visualization of MAM detections on 6 objects from the Object Segmentation Training Dataset. Blue dots represent object part activations from MPBP inference with MAMs. From the results we can see that, despite challenges like deformable objects, similar color to background, and adversarial surface properties (e.g. reflective), our object-specific MAMs do a good job at detecting the objects, and give interpretable decodings, which we can use to further understand the pose of the detected objects.

References

- [1] Miguel Lázaro-Gredilla, Yi Liu, D Scott Phoenix, and Dileep George. Hierarchical compositional feature learning. *arXiv preprint arXiv:1611.02252*, 2016.
- [2] Andy Zeng, Kuan-Ting Yu, Shuran Song, Daniel Suo, Ed Walker Jr, Alberto Rodriguez, and Jianxiong Xiao. Multi-view self-supervised deep learning for 6d pose estimation in the amazon picking challenge. In *Proceedings of the IEEE International Conference on Robotics and Automation*, 2017.